UNIVERSITY OF MINNESOTA
ST. ANTHONY FALLS HYDRAULIC LABORATORY
LORENZ G. STRAUB, Director

Technical Paper No. 28, Series B

Studies on Fluid Jets Discharging Normally into Moving Liquid

by
ROBERT L. GORDIER

August 1959
Minneapolis, Minnesota

UNIVERSITY OF MINNESOTA
ST. ANTHONY FALLS HYDRAULIC LABORATORY
LORENZ G. STRAUB, Director

Technical Paper No. 28, Series B

Studies on Fluid Jets Discharging Normally into Moving Liquid

by
ROBERT L. GORDIER

August 1959
Minneapolis, Minnesota

PREFACE

This report describes research which has been performed at the St. Anthony Falls Hydraulic Laboratory on jets impinging into a moving liquid. The work has been performed under contract Nonr 710(26) and this is the final report under that contract.

The project has been under the supervision of Professor E. Silberman to whom the writer is indebted for his advice in design and procedural matters as well as for the review of the report. Grateful acknowledgment is also expressed to the many members of the Laboratory staff who participated in preparing the experimental equipment, preparing the illustrations, and editing and publishing the report. Particular acknowledgment is expressed to H. Frederiksen and G. Subba Rao for their aid in collecting and reducing data. The study has been conducted under the general direction of Dr. Lorenz G. Straub, Director of the Laboratory.

A B S T R A C T

Results of tests on circular water and air-water mixture jets impinging normally into a water tunnel flow are given. Data taken on jet penetration are in agreement with results of previous experiments by others conducted in wind tunnels at jet-tunnel velocity ratios of six and less. A secondary effect is present at higher velocity ratios so that the penetration is deeper than previously indicated.

An empirical penetration parameter developed by the National Advisory Committee for Aeronautics [11] may be used for correlation of air-water mixture penetration data if the orifice is considered reduced in size by an amount equal to the area occupied by the air bubbles.

Entrainment of external flow is shown photographically. The studies indicate that entrainment from the wake of the jet proceeds in a periodic manner.

Total pressure data are in qualitative agreement with previous experiments conducted in wind tunnels. These show the characteristic kidney-shaped deformation predicted theoretically by Lu [3] and by Fraser [5].

An analysis of the two-dimensional or slot jet is presented for the case where the two flows are under the same total pressure. Comparison with penetration data on three-dimensional jets indicates that the rapid flattening of the jet gives it a quasi two-dimensional character.

C O N T E N T S

LIST OF ILLUSTRATIONS

LIST OF SYMBOLS

A - Area of orifice.

c - Contraction coefficient.

C_p - Total pressure coefficient - $C_p = \dfrac{p_T - 1/2\rho\, U_\infty^2}{1/2\rho\, [V_j^2 - U_\infty^2]}$.

C_s - Static pressure coefficient - $C_s = \dfrac{p - p_o}{1/2\rho\, U_\infty^2}$.

d - Orifice diameter.

d_w - Hypothetical orifice diameter reduced from the actual according to the air voids in an air-water mixture.

E_o - Total energy flux of jet at the orifice.

E_s - Total energy flux of jet in a section a distance s from the orifice.

F_x - Force exerted on the jet in the direction of the main stream.

g - Acceleration of gravity.

k - Pressure coefficient in the wake of a sphere - $k\,\dfrac{p_w - p_o}{1/2\rho\, U^2}$.

m - Velocity ratio, V_j/U_∞.

p_T - Total pressure.

p_o - Static pressure a long distance upstream.

p_s - Static pressure.

p_w - Wake pressure of sphere.

Q_a - Volume flow of air phase of jet fluid.

Q_j - Volume flow of jet liquid.

R - Gas constant.

s - Distance from the orifice along arc connecting points of maximum total pressure.

T - Temperature.

u - Velocity at a point.

U_∞ - Tunnel velocity.

v_s - Component of velocity perpendicular to traversing plane.

V_j - Jet velocity.

w_a - Specific weight of air.

w_j - Mean specific weight of jet fluid.

w_L - Specific weight of liquid.

W_a - Weight flow of air phase of air-water mixture.

W_L - Weight flow of liquid phase of air-water mixture.

x - Distance downstream from leading edge of orifice.

y - Deepest jet penetration at a distance x downstream.

z - One-half the maximum jet width at a distance x downstream.

ρ - Density of tunnel fluid.

ρ_j - Mean density of jet fluid.

STUDIES ON FLUID JETS DISCHARGING NORMALLY INTO MOVING LIQUID

I. INTRODUCTION

The penetrating ability and spreading of high velocity jets impinging into a moving liquid have proven of interest for a variety of reasons ranging from the production of underwater bubble screens to the cooling ability of air jets for turbo-jet engines. The behavior of submerged jets in a quiescent receiving liquid is quite well understood. With the aid of a single experimentally obtained constant, the complete mean flow pattern is derived analytically [1]. The jet undergoes lateral diffusion and deceleration and simultaneously accelerates and entrains external fluid into the jet. Analysis yields the distribution of volume, momentum, and energy flux downstream from slot and circular orifices; it is, however, based upon the two assumptions that the pressure is hydrostatic throughout and that similar velocity profiles exist at subsequent downstream sections [2].

When the receiving liquid moves at an angle to the jet flow, a force field is established about the jets and neither the assumption of hydrostatic pressure nor of similar velocity profiles can be made. Qualitatively, the jet may be likened to an obstruction in a uniform stream. The slot jet simulates a mound and the circular jet at the plane of efflux simulates a circular cylinder. A velocity field and corresponding pressure field are then established about the jet. This analogy is very rough, and because of flow entrainment and jet deformation in the three-dimensional case, the resulting flow pattern will be considerably different than that resulting from flow about a circular cylinder.

The research on which this report is based was undertaken to study the spreading of circular water and air-water mixture jets impinging into moving water. The objectives were to develop or to verify empirical relationships encompassing the physical properties governing the depth of penetration of the jet and lateral spreading of the jet, the latter being of importance in determining orifice spacing. Time limitations necessitated limiting the jet angle to 90 degrees. It was also intended to experimentally study the energy dissipation and to provide empirical relationships governing the rate of dissipation.

The present tests are apparently the first of this type to be carried out in a water tunnel; previous experimentation made use of wind tunnels. The water tunnel with dye jets facilitates visualization of the flow pattern because in a given range of Reynolds number much lower velocities are permitted than would be the case for wind tunnels. However, wind tunnels permit the use of hot-wire anemometers and generally facilitate physical measurements.

During the course of this study some time was devoted to an analysis of the two-dimensional jet with the thought of supplementing the data on the three-dimensional jets at least in a qualitative manner. The rapid flattening of the three-dimensional jet causes it to approach a two-dimensional case. A line of closely spaced orifices approximates the two-dimensional jet even better. It may be mentioned that the slot jet discharging into a moving fluid is in itself worthy of study because of its use in controlling circulation about air foils or hydrofoils, its potential in dissipating energy, and other special applications.

II. PREVIOUS WORK

A. Analytical Studies

A literature search has uncovered several references helpful to the objectives of this study. H. C. Lu [3] for his Ph.D. dissertation at Göttingen in 1942 undertook an analytical treatment of the three-dimensional jet impinging perpendicularly into a moving fluid. He reduced the problem to two dimensions by passing a series of closely spaced planes perpendicular to the jet axis through the jet. He considered the cylindrical stream a circular area of dead water in plane parallel flow. The problem was reduced to finding the surface of discontinuity between a parallel flow and a region of dead water as time moves on. He suggested two methods of solution, firstly by series and secondly by a system of successive approximations.

In the former method, he considered potential flow outside a dead jet area and also a second potential within the jet. Both potentials were expanded into a power series of a complex variable with coefficients given as functions of time. At the surface of discontinuity, the pressures of both flows were considered equal and opposite and the radial displacements equal. These boundary conditions permitted evaluation of the series coefficients by simultaneous solution of a system of equations. The computations are quite

involved, and in the numerical example cited, the analysis was valid only for values of time less than 0.6 sec because the radius ceased to be single valued for larger values of time. By this method, he succeeded in demonstrating the characteristic kidney shape acquired by the jet. To extend the analysis to larger values of time, he developed his method of successive approximations. This was based upon a numerical process for evaluating the induced velocities at the surface of discontinuity. His predicted jet shape is shown in Fig. 2b. Lu cited the wind-tunnel measurements of Bäuerle [4] which, he stated, showed the same geometrical pattern. A copy of the latter report was unavailable.

J. P. Fraser [5] suggested another method of numerical analysis. He assumed flow about a circular cylinder using actual pressure measurements based on laminar boundary-layer flow about a circular cylinder. He assumed a velocity potential to exist in the jet flow and no entrainment of external fluid. By applying the theory of small perturbations, he developed the velocity potential in series form with determinant coefficients. He also presented a rough method for predicting the penetration or turning of the jet based upon differential pressures. His numerical example indicated quite involved computations.

T. S. Walters [6] has published an article on the diffusion from an infinite line source lying perpendicular to the mean fluid flow. His analysis was for the case of smoke discharged from a line of stacks into the wind. Expressions were obtained for the distance downwind to the point where the ground-level concentration of the diffused smoke attained its maximum value. The condition of sources at ground level may be derived from this as a special example.

The two-dimensional jet directed at any angle, including 90 degrees, from either orifices or nozzles into a general stream, was treated by Ehrich [7]. Assuming the wake to be approximated by an extensive area of dead liquid, he applied the Helmholtz-Kirchhoff method of potential analysis and succeeded in determining the relationships between the geometrical and velocity parameters. He also provided an equivalent analysis for the case in which the trailing edge of the jet does not separate from the downstream wall. His study was necessarily limited to the condition that both jet and main stream were under the same total pressure. A common streamline with a continuous

velocity variation separates the two flows, and the jet and dead area wake are separated by a vortex sheet at uniform pressure. The review of this paper showed that Ehrich considered the velocity along the wake equal to the free stream velocity. Rationally, it would seem that this velocity would be higher because of the velocity field established about the obstructing jet. Based on this additional assumption, an analysis of the two-dimensional jet is treated in Appendix C.

G. I. Taylor [8] has suggested that the flow pattern about a high-velocity slot jet may be approximated by substituting a two-dimensional solid boundary for the jet.

B. Experimental Studies

Extensive studies in wind tunnels on the penetration of heated air jets into air streams have been conducted at the Lewis Flight Propulsion Research Laboratory of NACA. Air jets were introduced at considerably higher temperatures than the main flow, and the depth of penetration was sensed with a temperature rake. The original report [9] treated the effect of jet-to-main stream velocity and density ratios for circular jets. Subsequent reports treated the effect of orifice coefficient [10], efflux from square and elliptical as well as circular orifices [11], temperature profiles [12], and a general treatment of jets directed at various angles [13]. These data are used for purposes of comparison in the present report. It should be noted that the NACA tunnel was quite narrow in view of the rapid spreading of the jet.

Tests of air jets in wind tunnels relating to energy dissipation were conducted by Jordinson [14]. He provided considerable detailed data on total head contours of the spreading jet. His data are also used herein for purposes of comparison.

No reports of studies on air-water mixture jets impinging into a moving fluid were found in the literature.

Rouse [15] has presented data on the velocity and static pressure distribution in a two-dimensional jet. These data are cited in the treatment of the slot jet in Appendix C.

III. EXPERIMENTAL WORK

In the NACA research, it was found that jet penetration was dependent on the velocity ratio V_j/U_∞, the density ratio ρ_j/ρ and the diameter at the vena contracta, $\sqrt{c}\,d$. These symbols are defined as follows:

V_j = velocity in jet at efflux
U_∞ = tunnel velocity
ρ_j = jet fluid density
ρ = tunnel fluid density
c = coefficient of contraction for orifice

The plot of the NACA data on a co-ordinate system of $y/\sqrt{c}\,d$ versus the parameter

$$\frac{\rho_j V_j}{\rho U_\infty}\left(\frac{x}{\sqrt{c}\,d}\right)$$

showed little scatter over a considerable range in variables. Nevertheless, it was decided to repeat these tests with water jets discharging into water because it was felt worthwhile to increase the range of V_j/U_∞ and to find the influence of tunnel width, if any existed. Further, a Reynolds number effect was incorporated into the NACA parameters in a somewhat arbitrary manner by including it in the evaluation of the coefficient c. Tests on water jets emitted from nozzles should evaluate this treatment because the contraction is nonexistent and therefore independent of Reynolds number.

It was intended to attack the problem of energy dissipation in an empirical manner by taking total and static pressure readings about the jet. These data necessitated fabricating special instruments described under Section A below.

A. Experimental Apparatus

The gravity water tunnel used in these tests is shown photographically in Fig. 1. The tunnel cross section is 12 in. wide by 18 in. deep. A maximum velocity of 14 fps is available. In order to use the 18-in. dimension to optimum advantage, the orifices were located in the floor of the tunnel about 7 in. from the end of the contraction. River water was used in the

tunnel and tap water for the liquid component of jet flow. The tunnel flow was measured by a calibrated elbow meter which was checked by a total pressure survey. Water flow in the jet was measured by a calibrated orifice plate meter. Air-water jets were generated by connecting a compressed-air line to an aspirator in the water-jet line. Air flow was measured by an orifice plate meter and an air-water manometer. The state of the air was determined by making pressure measurements in an air-mercury manometer and measuring temperatures upstream of the orifice plates.

To insure steady flow to the orifice when dye was injected, a special piping arrangement was used. An aspirator was installed in the pipe line to the jet; this was connected through a three-way valve to overhead dye and constant-level water tanks. Either dyed water or clear water was added through this system at all times. When dye was cut in, very little fluctuation was noted in the jet flow manometer.

Except for the 3/8-in. thin-walled orifices, the orifices were 1 in. thick with bell-mouthed entrances. These will be referred to as either nozzles or thick-walled orifices.

To sense total and static pressures, a rake was designed that could be rotated and translated in the channel (Fig. 1). The rake head consisted of six total-pressure probes spaced at 1-in. intervals along one arm with two static probes mounted on the opposite arm. The rake enabled data to be obtained at several stations taken normally to the tunnel flow. In the vicinity of the orifice, where the jet flow was far from parallel to the tunnel flow, data were obtained by probing from the side of the channel with individual probes on planes parallel to and at 45 degrees to the plane of the orifice. Because of the curvilinear nature of the flow, it was necessary to design the probes to be relatively insensitive to angle of attack. A discussion of the sensing elements is presented in Appendix B.

B. Procedures

1. Spreading of the Jet

Data were taken from still photographs of colored water jets. The trajectories were enlarged by pantographing. Time averages were obtained by taking a number of photographs of each condition. As shown in Fig. 3, a mean curve was drawn through the resulting trajectories. Co-ordinates were taken

from this curve and plotted on the co-ordinate system given in NACA TN 2019, Fig. 3 [11]. At high jet velocities, the profile was outlined by injecting dye into the tunnel boundary layer upstream of the orifice since it was not feasible to inject dye into the high pressure jet system (see Fig. 3). The entrainment of boundary-layer dye proved to be a suitable method of marking the jet.

In addition to photographing the penetration trajectory, photographs were taken normal to the plane of the orifice to ascertain the lateral spreading.

The initial tests were conducted on a 1/2-in. diameter, bell-mouthed, thick-walled orifice, or nozzle. Discharge coefficient and density effects were accordingly eliminated and the resulting trajectories were simply a function of the velocity ratio. After evaluation of the velocity ratio effect, similar tests were run on a 3/8-in. diameter nozzle to evaluate the effect of size. Coefficient effects were studied by testing 3/8-in. diameter thin-walled orifices.

It was originally felt that air-water mixture jets would act as homogeneous liquid jets of reduced density and that their behavior could best be explained on the basis of the density ratio. Accordingly, the ratio of air to water in the jet flow was varied as well as the velocity ratio m. The air bubbles marked the jet suitably and dye was injected only to ascertain whether the air penetrated as far as the liquid.

2. Energy Dissipation

As the jet penetrates into the stream, it spreads, entrains external fluid, and rapidly decelerates. The surface of discontinuity separating the two flows is a vortex sheet across which the jet energy is rapidly dissipated. The jet is turned in the direction of the main stream. Ultimately, the two streams attain the same total pressure and the discontinuity ceases to exist. The total energy loss at exit becomes the difference between the jet total head and the stream total head measured at the point downstream where the flow is continuous. Assuming the stream flow to be large compared to the jet flow so that the energy loss in the main stream is negligible and assuming the static pressures in the two streams to be equal, the total loss per unit volume of jet fluid becomes

$$E_{total} = 1/2\rho(V_j^2 - U_\infty^2) \tag{1}$$

As in the case of a quiescent receiving liquid, this exit loss is not a local energy conversion. External fluid is accelerated and partly entrained while jet fluid is decelerated. Eddies generated by high shear cause the jet to deform and spread. Ultimately, the energy is dissipated by eddy viscosity.

By definition, the energy flux transported across any incremental area is the product of the total pressure, normal velocity, and incremental area. The flux transported across any plane may be ascertained by numerical integration if the data can be obtained experimentally.

The jet energy still available at any point a distance s from the orifice will be defined as the positive difference between the energy available at the point s and that of infinity. Thus, the total energy flux of the jet crossing any section such as a-a in Fig. 7 becomes

$$E_s = \sum [(p_s + 1/2\rho\, u_s^2) - (p_o + 1/2\rho\, U_\infty^2)]\, v_s \Delta A \tag{2}$$

in which p_s represents the local static pressure,
p_o represents the static pressure a long distance upstream,
v_s represents the local velocity normal to the plane a-a,
u_s represents the local absolute magnitude of the velocity, and
ΔA represents a local incremental area.

The ratio of the jet energy available to the total jet energy becomes

$$\frac{E_s}{E_o} = \frac{\sum [(p_s + 1/2\rho\, u_s^2) - (p_o + 1/2\rho\, U_\infty^2)]\, v_s \Delta A}{[(1/2\rho)(V_j^2 - U_\infty^2)]\, Q_j} \tag{3}$$

Adopting Jordinson's [14] definition of the total pressure coefficient, this becomes

$$\frac{E_s}{E_o} = \frac{\sum C_p\, v_s \Delta A}{Q_j}$$

in which C_p is given by the ratio of the quantities in brackets in Eq. (3).

It is noted that the definition given prior to Eq. (2) defines the limits of the jet as the zone of positive total pressure. However, a zone of negative total pressure occurs in the wake. This is a consequence of the main flow about the jet. The jet exerts a retarding force on the stream equal and opposite to the force exerted in turning the jet and accelerating it in the direction of the stream. For the normally directed jet, this is given by

$$F_x = \rho Q_j U_\infty \tag{5}$$

Summation of Eqs. (3) or (4) across the whole plane may plausibly result in negative energies. Applying the above definition restricts and defines the jet limits as the outermost contour of positive total pressure.

It was intended originally to experimentally evaluate Eq. (4) for various m ratios and to determine an empirical relationship between E_s/E_o and the distance s along the maximum-velocity arc. Difficulties in obtaining static pressures and flow directions near the plane of efflux ultimately rendered this evaluation unfeasible.

IV. RESULTS AND DISCUSSION

A. Jet Penetration

A comparison of the jet penetration data taken for the 1/2-in. thick-walled orifice with that given in NACA TN 2019 is shown in Fig. 4a. A definite velocity ratio effect is apparent. For values of the velocity ratio m, less than six, the data are in good agreement; this is in accord with the original NACA study in which the m values were limited to about five [9]. In subsequent NACA studies when the m value was increased to approximately eight, a Reynolds number correction was introduced. The original co-ordinate system was modified by using the diameter of the jet at the vena contracta and empirically evaluating the contraction coefficient as a function of Reynolds number [10, 11]. In other words, the co-ordinate system was modified to accommodate an apparent Reynolds number effect. The coefficient of the nozzle in the present studies is unity and the concept of a contraction coefficient dependent on Reynolds number is inapplicable. Further, the present tests run at varying velocity ratios, but at constant jet velocity, indicated the effect

was a secondary velocity ratio effect rather than a Reynolds number effect.

The present tests were conducted over a range in jet Reynolds number from 70,000 to 250,000 and are well within the range of the NACA tests. The velocity ratios of the jet to stream were extended beyond previous experiments and a penetration deeper than expected was noted at high ratios. The correlating parameter is the velocity ratio itself rather than the Reynolds number.

Figure 4b shows an overall plot including data from the 3/8-in. thick- and thin-walled orifices. A coefficient of 0.630 was used for the thin-walled orifice and unity was used for the others. The range in jet velocities was from approximately 15 to 79 fps and channel velocities were varied from 4 to 10 fps. Although the data from the 3/8-in. thin-walled orifice are in qualitative agreement with the nozzle data, the penetration is deeper than would be expected. It is noted that the dashed curve at $m = 15$ representing data from the thin-walled orifice falls above the position that would be expected by extrapolation.

As stated above, the air-water jets were initially considered jets of a homogeneous fluid of lesser density. This plot on the co-ordinate system given in [10] is shown in Fig. 5a. The mean specific weight of the jet is given by

$$w_j = \frac{W_L + W_a \nearrow^0}{Q_L + Q_a} \approx \frac{W_L}{W_L/w_L + W_a/w_a}$$

The jet-stream density ratio becomes

$$\frac{\rho_j}{\rho} = \frac{w_j}{w_L} = \frac{W_L/w_L}{W_L/w_L + W_a/w_a} = \frac{Q_L}{Q_L + Q_a} \qquad (6)$$

and $w_a = \dfrac{R/T}{p}$

where w = specific weight,

w_j = mean specific weight of jet fluids,

W = weight flow in pounds per sec,

Q = volume flow in cfs,

R = gas constant in ft per degree Rankine,

T = temperature in degrees Rankine, and

ρ_j = mean specific weight of jet fluids.

Subscripts L and a refer to liquid and air respectively.

Considering the product of the first two components of the NACA parameter

$$\frac{\rho_j}{\rho} \frac{V_j}{U_\infty} \sqrt{\frac{x}{c\,d}}$$

it can be shown that the penetration is a function only of the liquid flow and nozzle size as follows:

$$\frac{\rho_j}{\rho} \frac{V_j}{U_\infty} = \frac{Q_L}{Q_L + Q_a} \frac{Q_L + Q_A}{1/4\pi\, d^2} \times \frac{1}{U_\infty} = \frac{Q_L}{U_\infty A} \tag{7}$$

The implication here is that the penetration depends only on the volumetric flow of water in the jet and is independent of velocity. The spread of data and lack of co-ordination in Fig. 5a indicate that this is not the case and that the air-water mix jet cannot be treated as a homogeneous fluid.

Noting that the penetration depends in some way on the momentum of the water phase of the jet and that air momentum is negligible, the parameter may be modified by considering only the water flow through a reduced orifice.

$$A_w = \frac{Q_L}{V_j} = \left(\frac{Q_L}{Q_L + Q_A} \right) A$$

$$d_w = \left(\sqrt{\frac{Q_L}{Q_L + Q_A}} \right) d \tag{8}$$

The equation of the trajectory is modified by substituting d_w for d. Hence

$$\frac{y}{d} = f\left(\frac{\rho_j}{\rho}\frac{V_j}{U_\infty}\sqrt{\frac{x}{d}}\right) \quad \text{becomes}$$

$$\left(\sqrt{\frac{Q_L + Q_a}{Q_L}}\right)\frac{y}{d} = f\left[\left(\frac{V_j}{U_\infty}\right)\left(\frac{Q_L + Q_a}{Q_L}\right)^{1/4}\sqrt{\frac{x}{d}}\right] \tag{9}$$

or

$$\frac{y}{d_w} = f\left(\frac{V_j}{U_\infty}\sqrt{\frac{x}{d_w}}\right) \tag{10}$$

Figure 5b shows a plot of the same data on this modified co-ordinate system. Comparison with the water-jet data shows the penetration may again be described by a family of curves with the m ratio being the parameter. It is noted, however, that the data fall somewhat above the original curves. This may indicate a buoyant effect. It was originally felt that buoyancy would be insignificant in the initial turning of the jet. It was reasoned that the air with negligible mass would quickly respond to side pressures with a resulting separation of the water and air components. Dye injected into the jet showed no such separation and the air bubbles appeared to penetrate as deep as the colored water. Virtual mass and drag effects on the bubbles are undoubtedly important considerations in this respect.

In Figs. 4 and 5, x is measured from the upstream side of the orifice rather than the centerline as was done in the NACA tests. The latter data were taken at abscissa values greater than ten and the effect of the slight change in the origin is negligible beyond this value of the parameter.

B. Lateral Spread of the Jet

In Fig. 6 typical photos taken normal to the plane of the orifice are shown. These photos were pantographed and the data correlated in a manner similar to the handling of the penetration data. It was determined empirically that the spread of the jet could be expressed by the relationship

$$z/d = 0.6\ V_j/U_\infty (x/d)^{.39} \tag{11}$$

in which z represents 1/2 the maximum width of the jet at a distance x downstream. Figure 6 shows a plot of the data and this mean curve.

It should be noted that this relationship is based on somewhat scanty data and is only valid for m values less than eight. Only photos of colored water jets from thick-walled orifices were included.

It is appreciated that the spreading and penetration of the jet were determined in a statistical manner and are subject to errors resulting from too few samples. These data were based on the mass concentration boundary. The NACA data were obtained from the thermal boundary. Since thermal mixing proceeds at about the same rate as mass mixing, the data should be comparable.

C. Energy Dissipation

Total and static pressure traverses were conducted at several stations along the tunnel for m values of four, six, and eight. Location sketches for the cross sections traversed are shown in Fig. 7. The trajectories of lines connecting points of maximum total pressure are also shown in the figure and are compared with Jordinson's data [14]. For values of $x/d < 17$, these data approximate the curve

$$y/d = 1.31\,[V_j/U_\infty \sqrt{x/d}]^{.74} \qquad (12)$$

No ready explanation is apparent for the discrepancy between Eq. (12) and Jordinson's curves except that the zone of positive total pressure becomes quite flat as the distance from the orifice is increased. A slight change in total pressure reading resulting from differences in the degree of turbulence in the tunnels could result in a considerable shift in position of the point of maximum total pressure.

However, in Fig. 7, Eq. (12) is used and the relationship between distances measured along the curves for various m values and the velocity ratio

$$\frac{u_{max} - U_\infty}{V_j - U_\infty}$$

is shown. A comparison is also provided for the case of the quiescent receiving

fluid, i.e. $m \rightarrow \infty$. In the latter case, the orifice velocity is maintained for a distance of 6.2 diameters. The graph indicates that this distance decreases with decreasing m ratios. It should be noted that near the orifice it is difficult to pick up the maximum readings because of the extreme variations in velocity over a small area. The probe dimensions (see Fig. B-2) are too large to be considered point readings and the average over an area will likely be low.

Velocity and static pressure data taken at stations on the tunnel centerline are shown in Fig. 8. These show the rapid deceleration of the jet and the zone of negative pressure which develops in the wake.

Figures 9, 10, and 11 show the total pressure and some static pressure contour data. A complete comparison with Jordinson's total pressure data is left to the reader. The former data showed a consistent zone of higher negative readings extending to the plane of the orifice. Other conflicts are present in magnitudes of total pressures and spread of the jet. These perhaps result from the relatively high degree of turbulence present in the water tunnel. Suffice it to say that the two sets of data are in qualitative agreement particularly concerning the kidney shape of the jet.

The positive total head contours show that energy is dissipated at a higher rate as the tunnel velocity is increased (or the m ratio decreased). Insufficient positive readings were sensed for $m = 6$ to trace the jet 17 diameters downstream. For the same station at $m = 4$, no trace of the jet could be noted and the readings were primarily negative.

The negative total pressure zone represents the energy lost in the main stream in turning the jet. Energy is brought into this zone by turbulent mixing. This results in an apparent energy recovery with distance only because losses to the external fluid were too slight to measure.

The static pressure contours are given only for qualitative reasons. In the plane traversed near the orifice, the fluctuating nature of the flow made accuracy impossible with the instrumentation used. Attempts to visually obtain flow direction with pieces of yarn attached to a probe showed extreme fluctuations in the neighborhood of the jet. Readings were discarded near the center of the jet and it should be noted that the data shown are subject to error. It is noted that negative pressures exist even on the stagnation side of the jet for $m = 8$. At $m = 6$, slight positive pressures were noted on the

upstream side. At $m = 4$ (data not shown), a considerable zone of positive pressure at higher coefficient values exists about the jet except in the wake.

If the flow near the orifice is likened to the flow about a circular cylinder, progressively higher positive pressures would be expected as the orifice is approached from the upstream side. Further, at any given upstream point, the pressure may be expected to be independent of the jet velocity and dependent only on the stream velocity. The static pressure data do not support such an argument. This anomaly may be explained qualitatively by noting that the entraining power of the jet which is a function of its velocity, or more accurately, the m value, accelerates the external flow in a manner akin to a sink. The resulting drop in pressure opposes the stagnation effect of the jet. At high m values, a negative static pressure results and at low m values a positive pressure results upstream of the orifice. The static pressure contour data shown as well as bottom static readings substantiate this. It was not feasible to locate a bottom pressure tap closer than 1-1/4 diameters from the upstream lip of the orifice. Static pressure coefficients C_s increased from -.19 for $m = 8$ to +.09 for $m = 4$ at this point.

Undoubtedly, stagnation exists on the upstream edge of the orifice. At high m ratios, this is limited to a very small zone. Figure 12 shows a comparison of flow entrainment at m ratios of 8 and 15.4, the former jet issuing from a 1/2-in. diameter nozzle and the latter from a 3/8-in. thin-walled orifice. In each case, dye is shown being injected into the tunnel boundary layer upstream of the jet. A definite zone of stagnation is apparent about the slower moving jet and the dye flows around the jet and is entrained in the wake. The phenomena are seemingly contradictory in that the entrainment into the higher speed jet is from the upstream side. In this case, stagnation must be limited to a small zone and flow is apparently entrained from all sides.

Figure 12 also shows dye being injected into the boundary layer in the wake of the jet. The dye is partially entrained into the jet. The action proceeds in a definite periodic manner. This is seen from the bands of dye in the still photo shown but is more graphic in motion pictures of the entrainment.

V. CONCLUSIONS

(1) Tests conducted in a water tunnel verified the NACA penetration data at jet-channel velocity ratios less than six. At higher values, a secondary effect other than jet Reynolds number is present to cause deeper penetration than previously predicted.

(2) Air-water mixture jets may be correlated by the NACA penetration parameter if the water phase only is considered as issuing from an orifice of area reduced according to the air void area.

(3) The maximum lateral spread of liquid jets discharging into the same liquid is approximately given by

$$z/d = 0.6\ V_j/U_\infty (x/d)^{.39}$$

in which z represents one half the maximum jet width at a distance x downstream for $m \leq 8$.

(4) When the jet impinges into a moving stream, a pressure field is established about the jet. This pressure field, as evidenced by the total pressure contour plots, causes the jet to bend and to deform into the characteristic kidney shape predicted by Fraser and Lu (see Fig. 2b).

(5) The rapid flattening of the jet gives it a quasi two-dimensional character at $m = 1$. The actual penetration trajectory for a circular jet at this m ratio falls surprisingly close to the theoretical trajectory of the slot jet.

(6) The pressure field is dependent on the velocity ratio such that at low m values flow is entrained only from the wake whereas at high m values, flow is apparently entrained from all sides of the jet.

(7) Wake fluid is entrained into the jet in a periodic manner.

LIST OF REFERENCES

[1] Albertson, M. L., Dai, Y. B., Jenson, R. A., and Rouse, H. "Diffusion of Submerged Jets," Transactions ASCE, Vol. 115, pp. 639-664. 1950.

[2] Holdhusen, J. S. "Discussion of Diffusion of Submerged Jets," Transactions ASCE, Vol. 115, pp. 665-667. 1950.

[3] Lu, H. C. On the Surface of Discontinuity Between Two Flows Perpendicular to Each Other, Nat. Tsing Hua Univ. Eng. Report, 4, 1, pp. 40-62. October 1948.

[4] Bäuerle, H. Obliquely Blown Jets, (A discussion of work by H. Bäuerle), M. A. P. Volkenrode. AVA Monogram J_2 4.31.

[5] Fraser, J. P. "Three Dimensional Study of a Jet Penetrating a Stream at Right Angles," Journal of the Aeronautical Sciences, Vol. 21, pp. 59-60. January 1954. See also MS thesis, Cornell University.

[6] Walters, T. S. "Diffusion from an Infinite Line Source Lying Perpendicular to the Mean Wind Velocity of a Turbulent Flow," Quarterly Journal of Mechanics and Applied Mathematics, Vol. 10, No. 2, pp. 214-219. May 1957.

[7] Ehrich, F. F. "Penetration and Deflection of Jets Oblique to a General Stream," Journal of the Aeronautical Sciences, Vol. 20, pp. 99-104. February 1953.

[8] Taylor, G. I. The Use of a Vertical Air Jet as a Wind Screen. Memoires sur la Mécanique des Fluides, Ministere de l'Air, pp. 313-317. 1954.

[9] Callaghan, E. E. and Ruggeri, R. S. Investigation of the Penetration of an Air Jet Directed Perpendicularly to an Air Stream. NACA TN 1615, 13 pages. June 1948.

[10] Callaghan, E. E. and Bowden, D. T. Investigation of Flow Coefficients of Circular, Square, and Elliptical Orifices at High Pressure Ratios. NACA TN 1947, 25 pages. September 1949.

[11] Ruggeri, R. S., Callaghan, E. E., and Bowden, D. T. Penetration of Air Jets Issuing from Circular, Square, and Elliptical Orifices Directed Perpendicularly to an Air Stream. NACA TN 2019, 18 pages. February 1950.

[12] Callaghan, E. E. and Ruggeri, R. S. A General Correlation of Temperature Profiles of a Heated Air Jet Directed Perpendicularly to an Air Stream. NACA TN 2466, 37 pages. September 1951.

[13] Ruggeri, R. S. General Correlation of Temperature Profiles Downstream of a Heated Air Jet Directed at Various Angles to Air Stream. NACA TN 2855, 59 pages. December 1952.

[14] Jordinson, R. Flow in a Jet Directed Normal to the Wind. Reports and Memoranda, No. 3074, Aeronautical Research Committee (Great Britain), 17 pages. October 1956.

[15] Rouse, H. Diffusion in the Lee of a Two-Dimensional Jet. Extracts of Proceedings, Ninth International Congress of Applied Mechanics, University of Brussels, Vol. 1, pp. 307-315. 1957.

[16] Winternitz, F. A. L., and Hopkins, D. Simple Total Pressure Probes with Spherical Shields. DSIR, Mechanical Engineering Laboratory (Great Britain), 26 pages. January 1958.

A P P E N D I X A

Figures 1 through 12

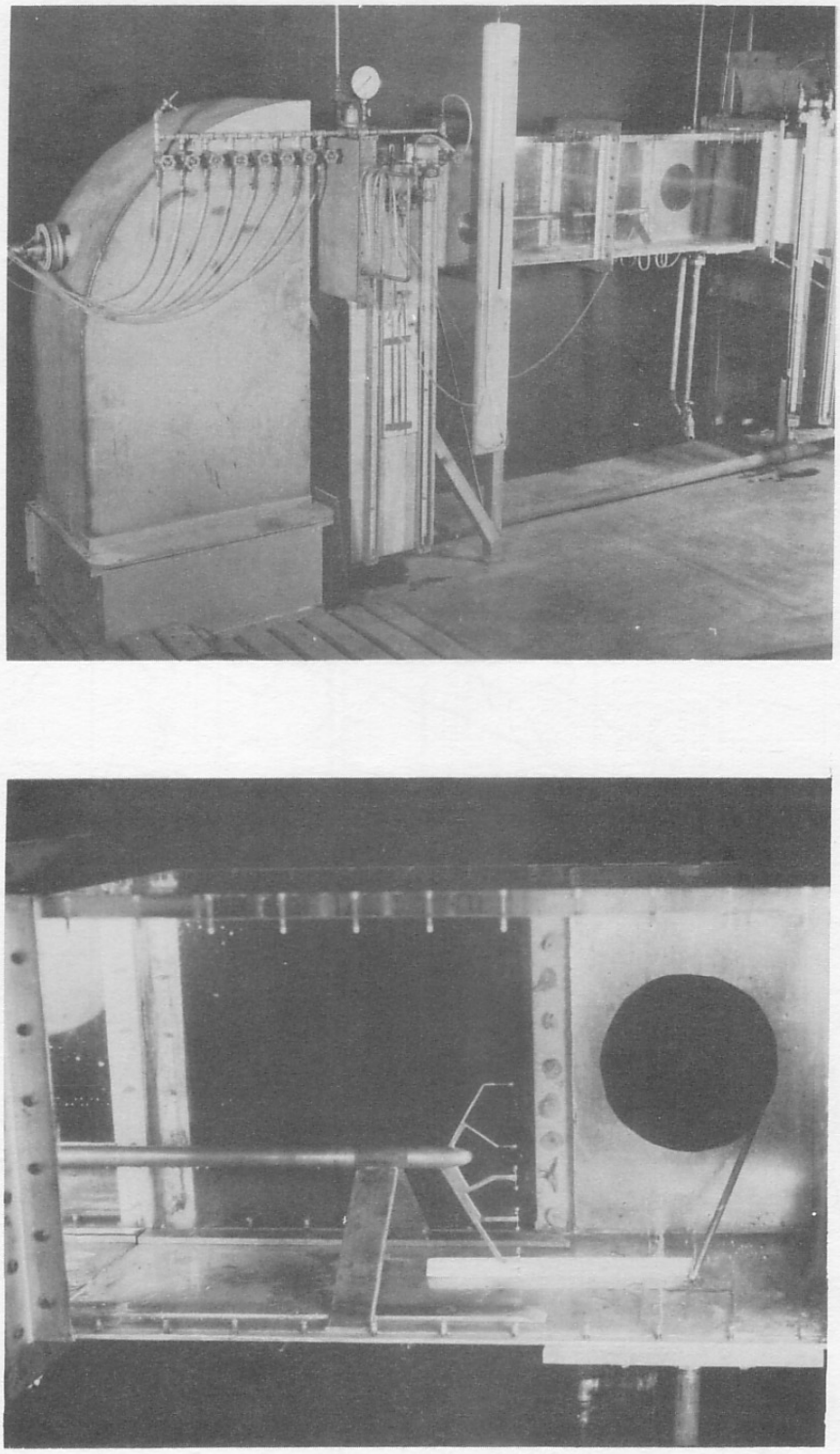

Fig. 1 – Gravity Water Tunnel and Probe Rake

a.- Typical Air-Water Mixture Jet

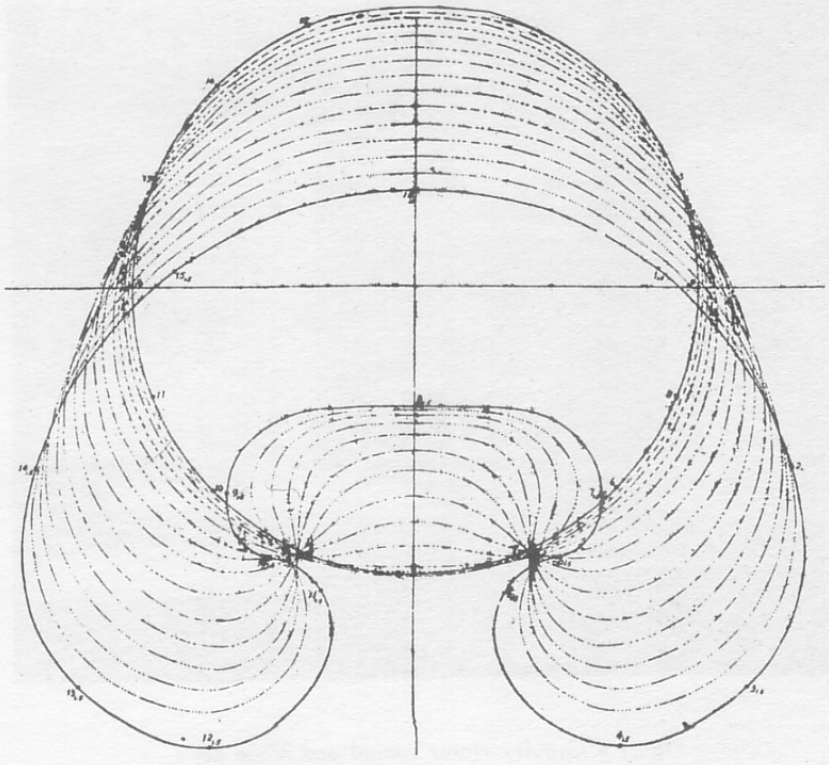

b.- Theoretical Prediction by H. C. Lu taken from Reference [3]

Fig. 2 - Jet Deformation

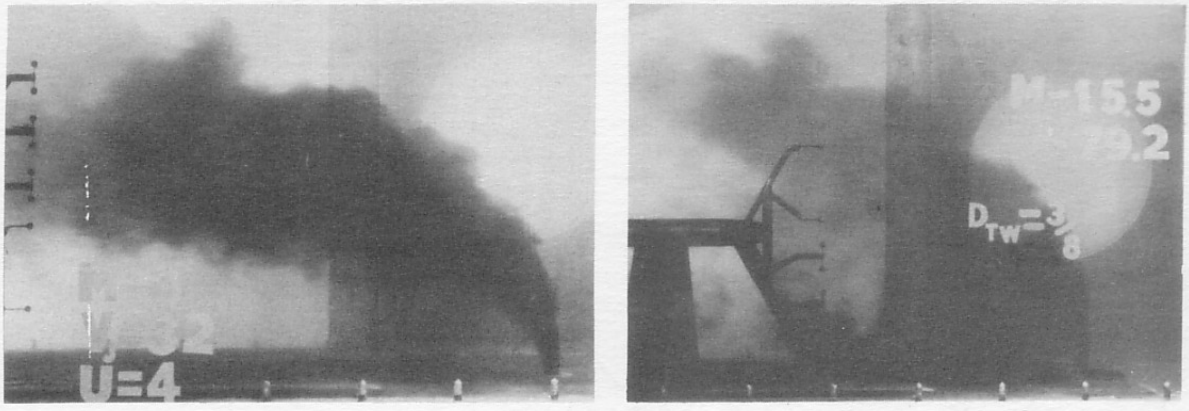

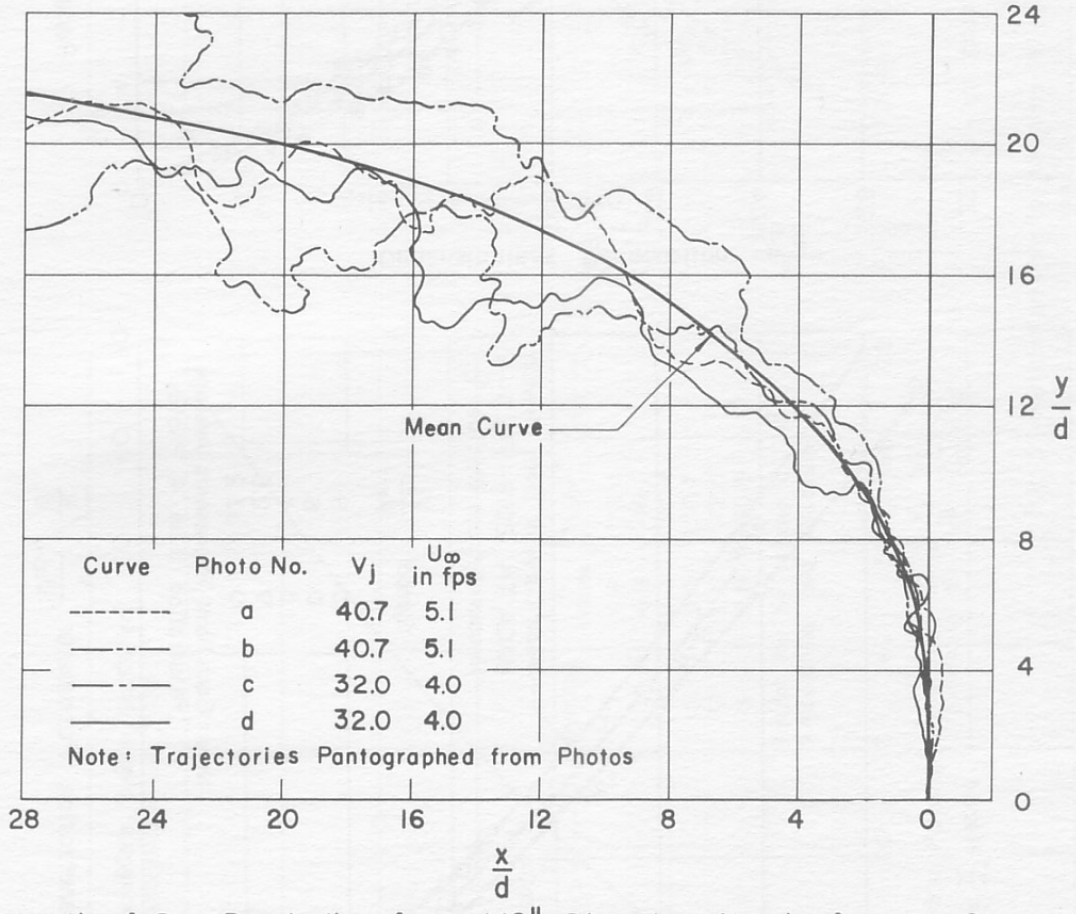

Depth of Dye Penetration from 1/2" Diameter Nozzle for m = 8

Fig. 3 - Typical Jet Penetration Trajectories

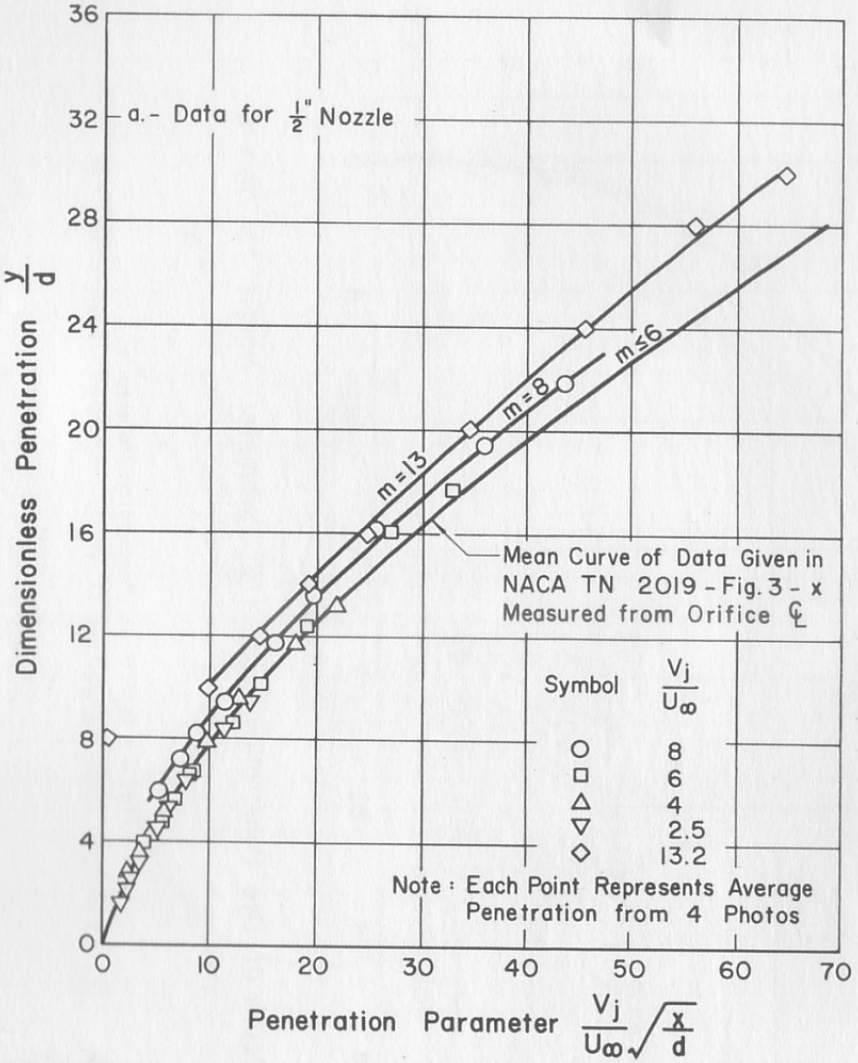

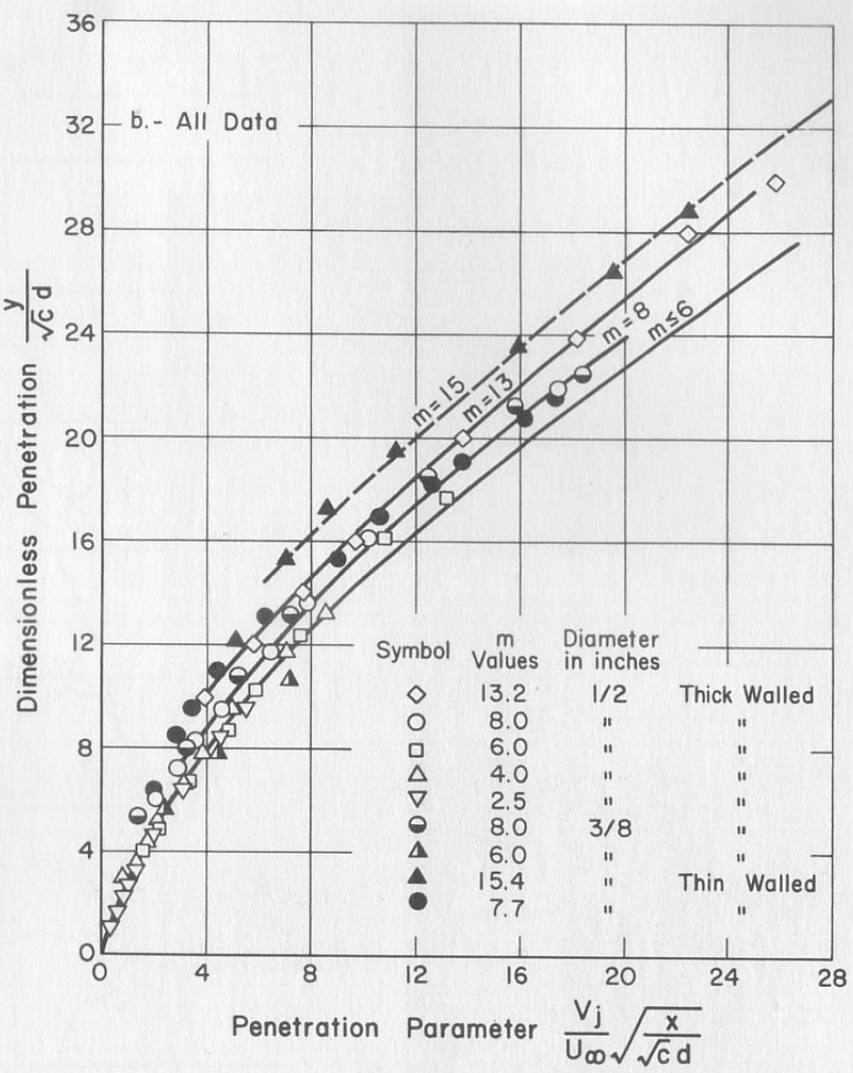

Fig. 4 - Penetration Data for Colored Water Jets

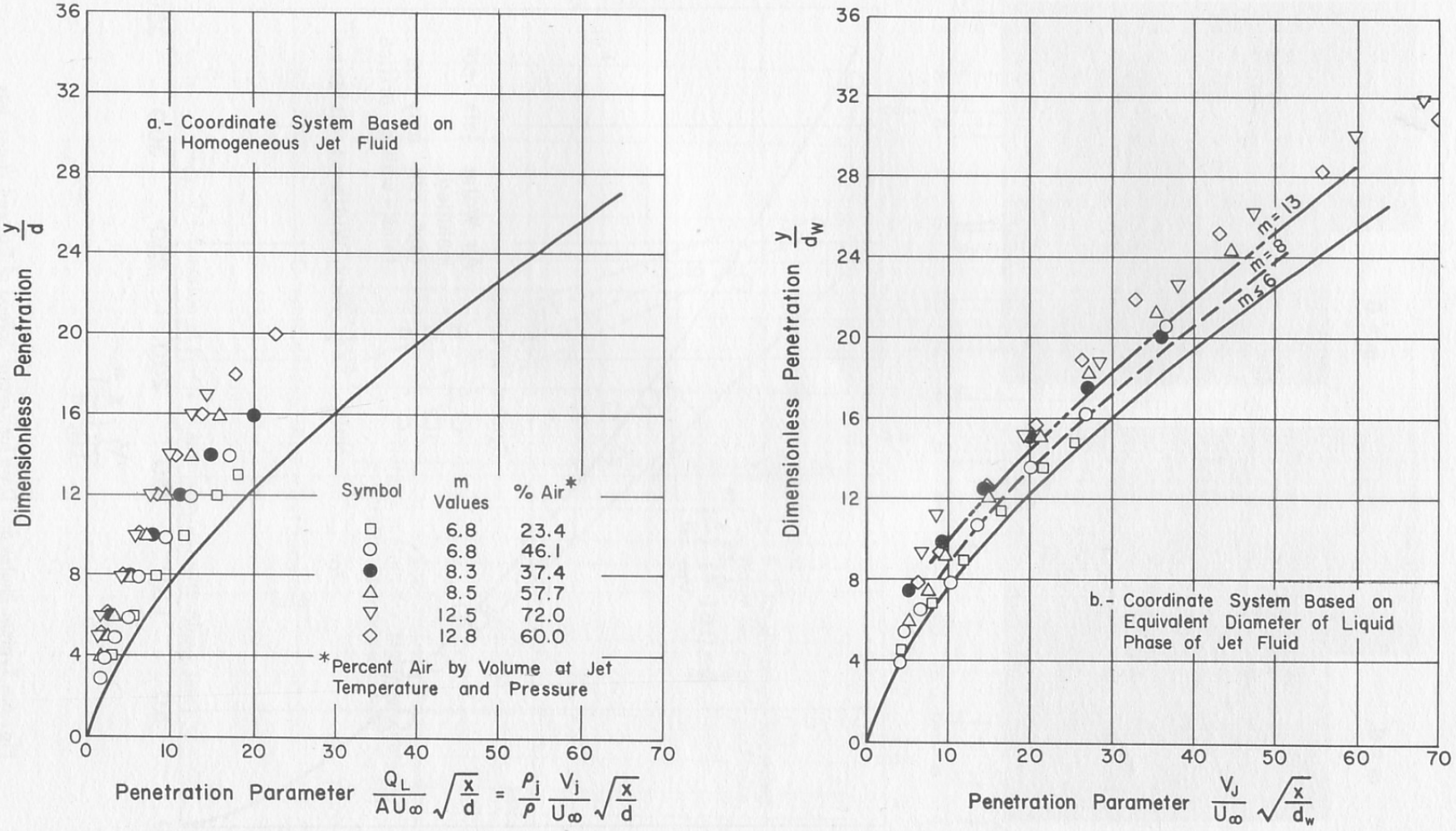

Fig. 5 - Penetration Data for Air-Water Mixture Jets

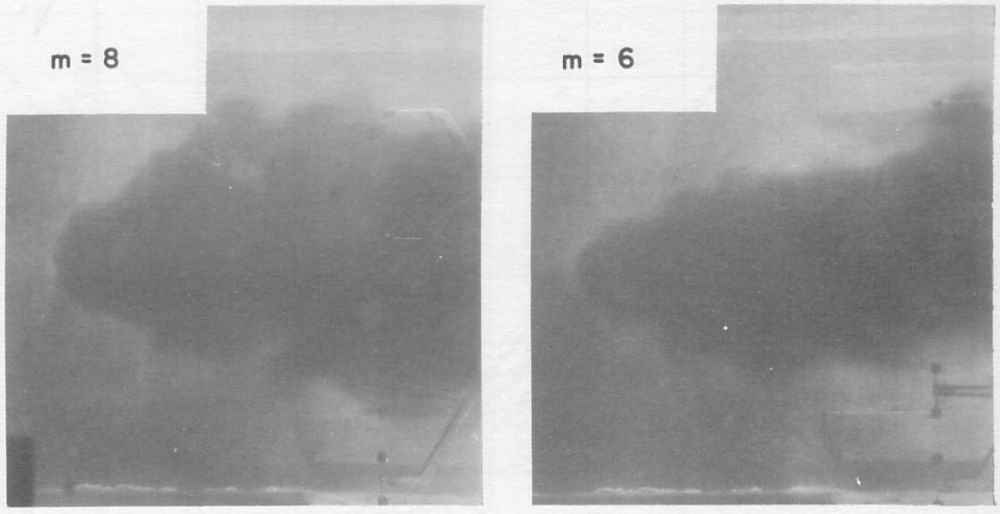

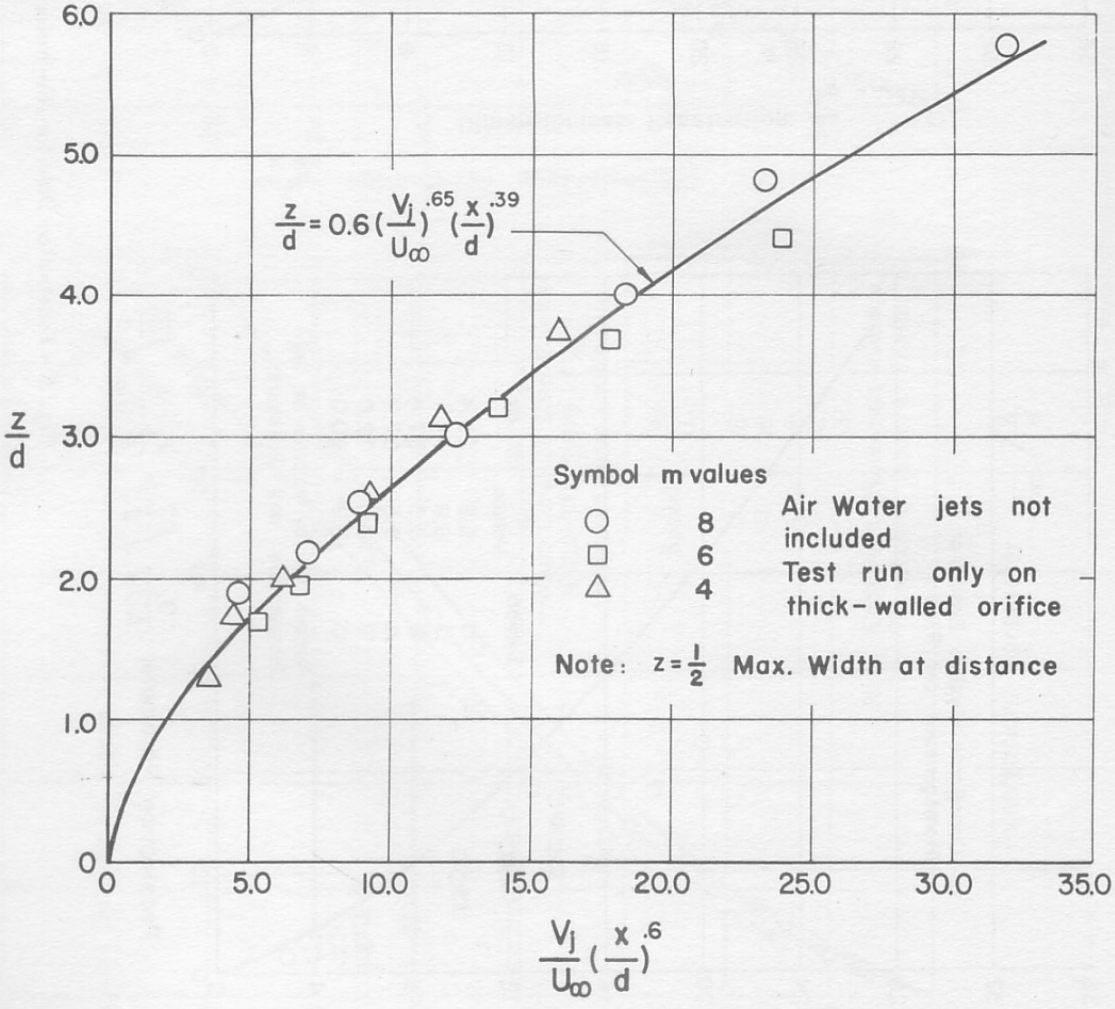

Fig. 6 - Typical Photos and Data for Lateral Spread of Colored Water Jets

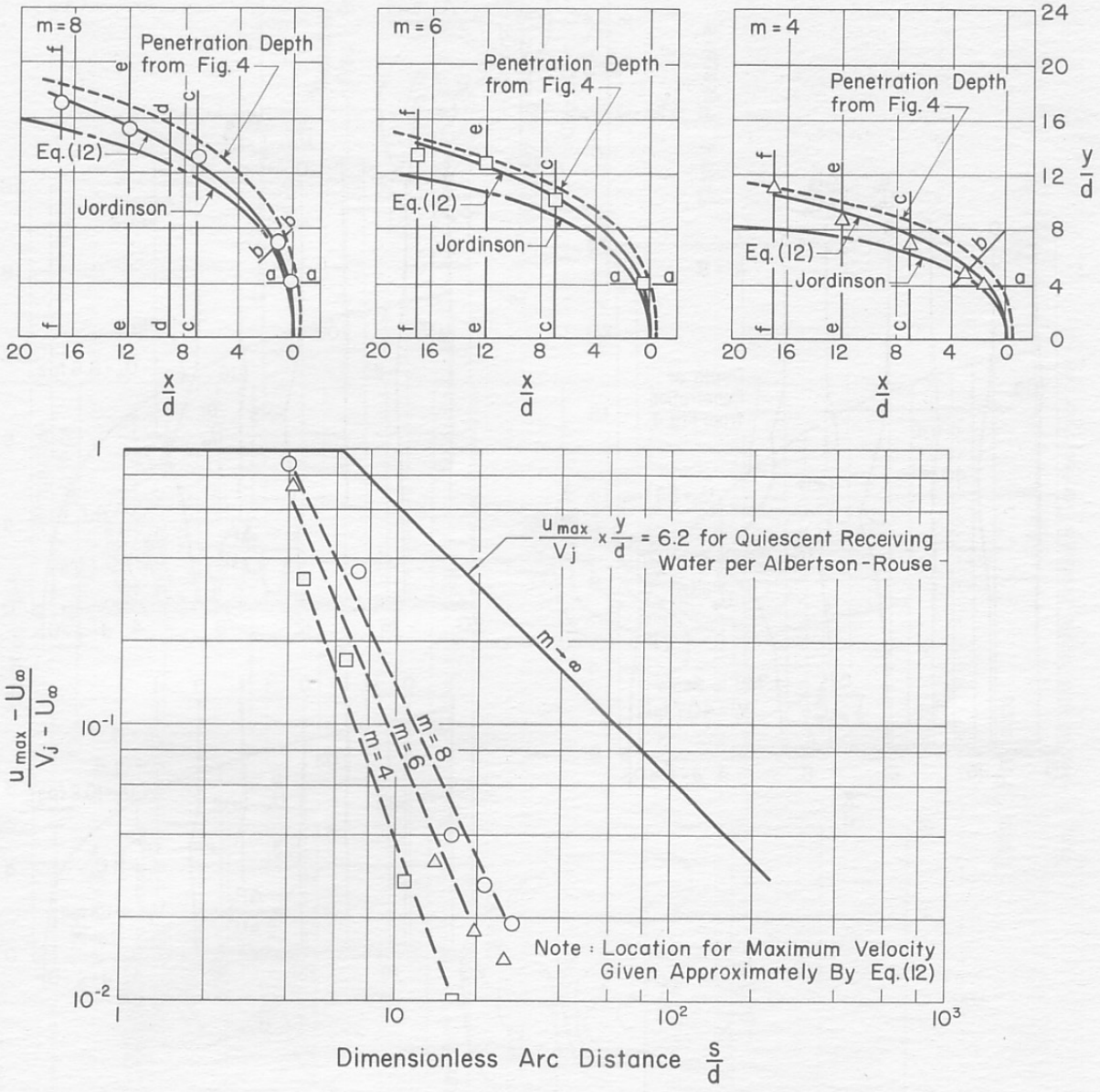

Fig. 7 - Location of Points of Maximum Velocity Along Jets

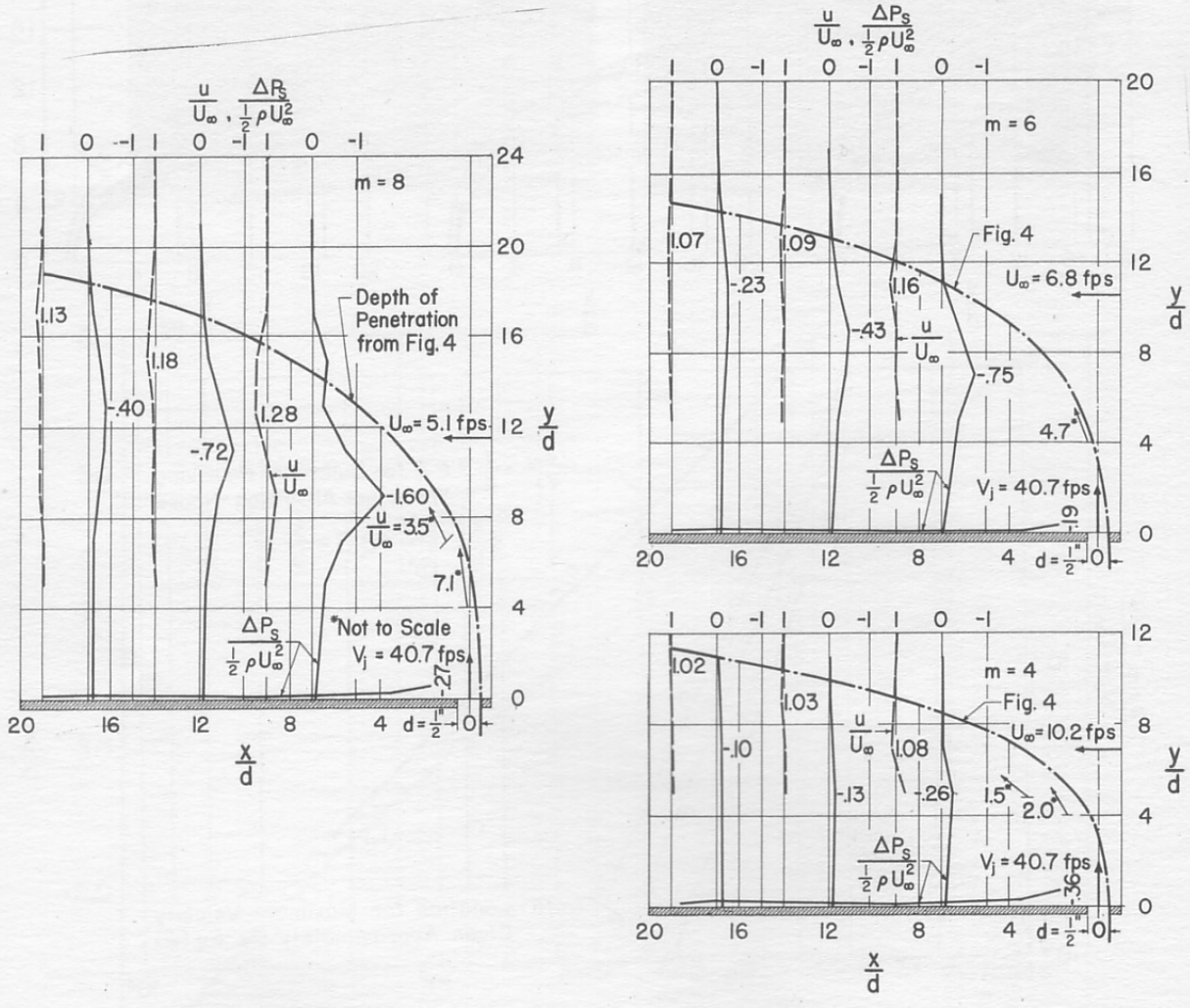

Fig. 8 – Static Pressures and Velocities on Plane of Symmetry for Several m Ratios

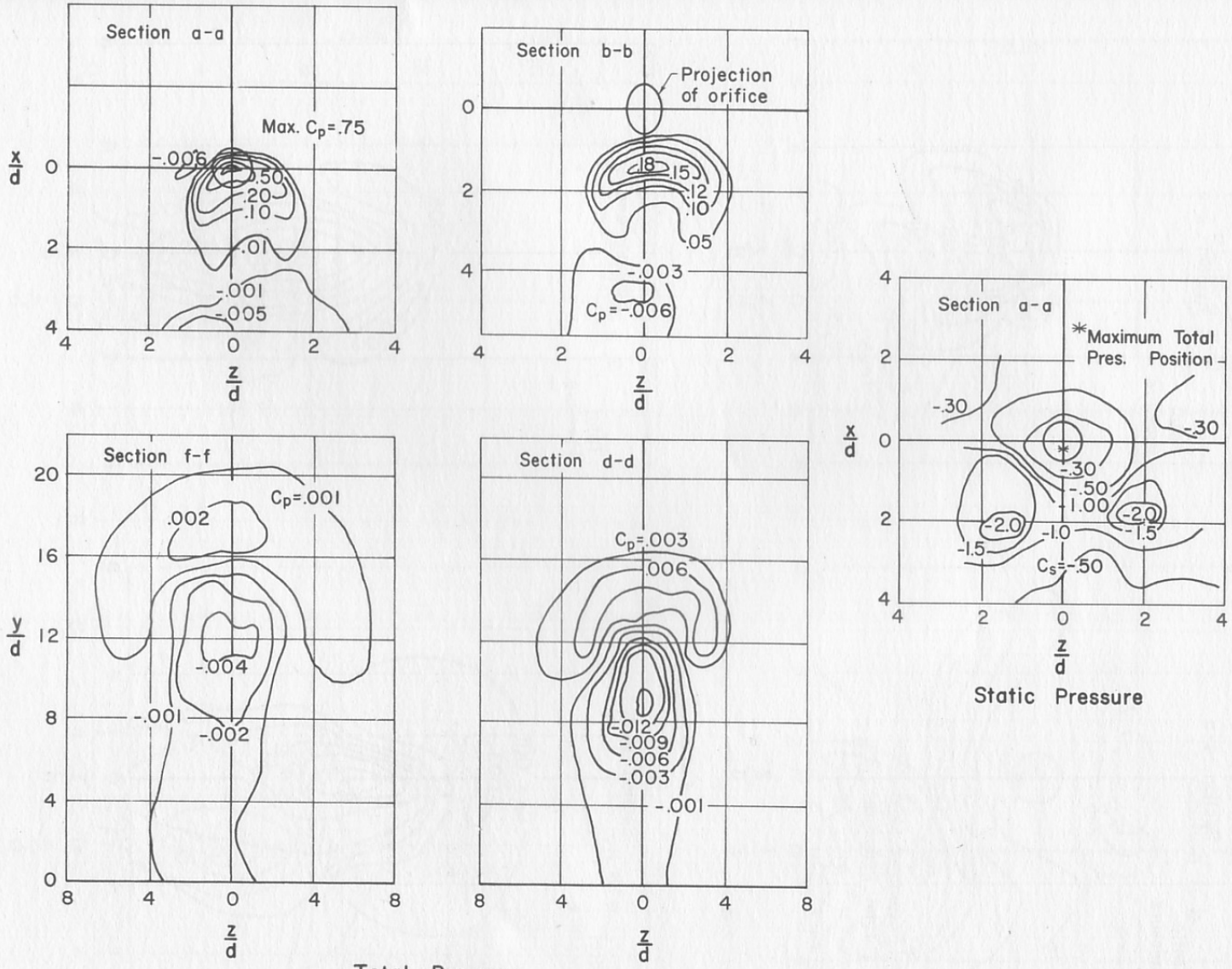

Fig. 9 - Total and Static Pressure Contours for m = 8

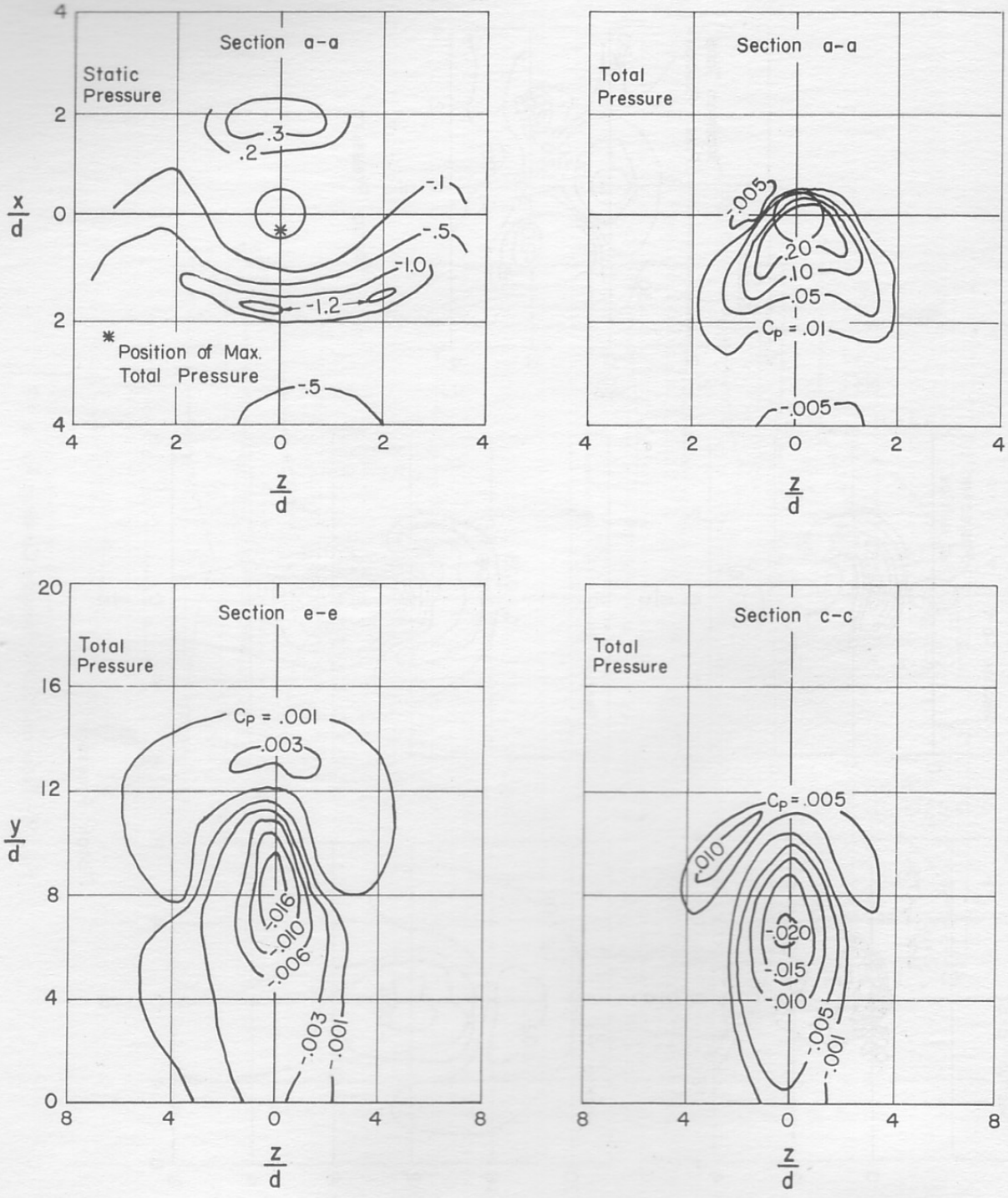

Fig. 10 – Total and Static Pressure Contours for m = 6

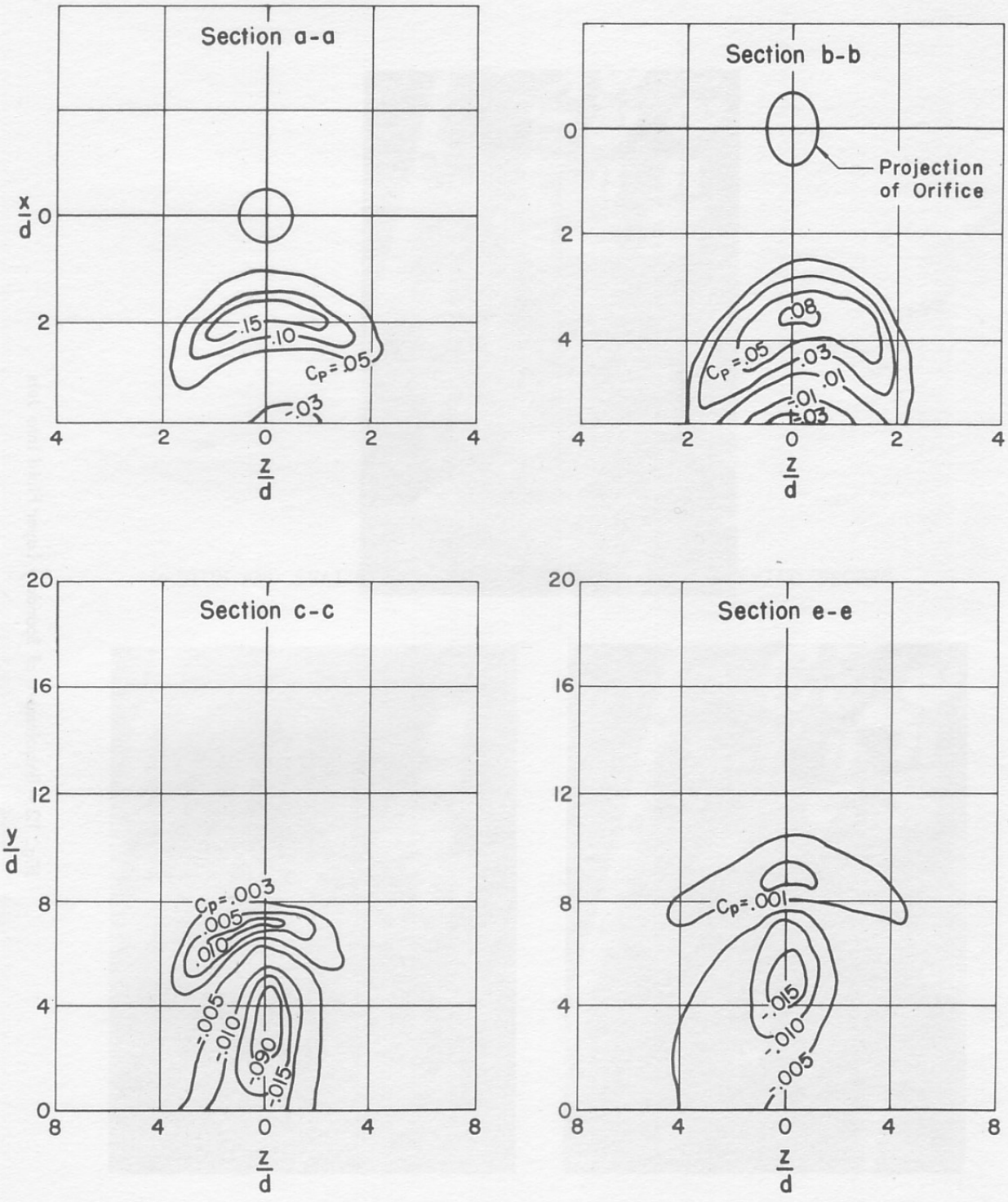

Fig. 11 - Total Pressure Contours for m = 4

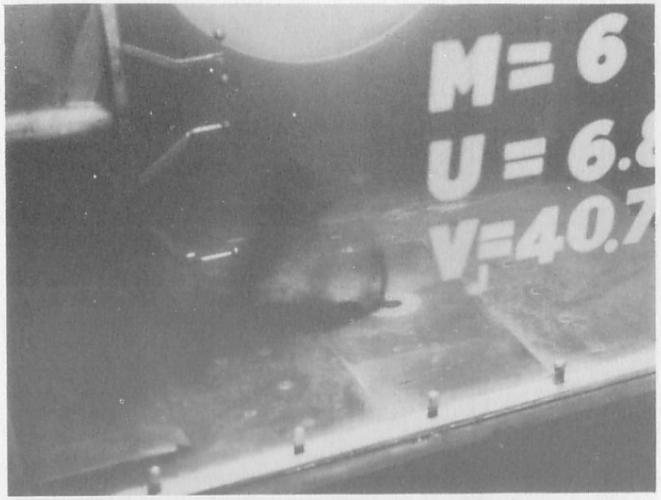

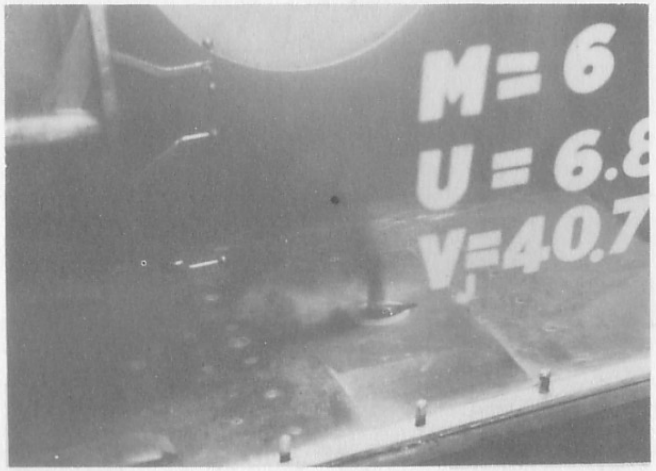

Fig. 12 – Entrainment of Boundary Layer Fluid into Jets

APPENDIX B

DESIGN AND EVALUATION STUDIES FOR PRESSURE SENSING PROBES

APPENDIX B

DESIGN AND EVALUATION STUDIES FOR PRESSURE SENSING PROBES

Winternitz and Hopkins' report [16] was followed in designing the total pressure elements. The probe given in their Fig. 9B was followed except that 1/4-in. diameter brass balls were used rather than the 0.300-in. balls they specified. The other dimensions were reduced proportionately. The rake and individual probes are shown photographically in Fig. B-1. Probe dimensions and results of evaluation tests conducted on the individual probe are shown in Fig. B-2a. This probe was modified by boring out the venting hole to twice the size; the former probe was used on the rake, the latter for individual probing. Evaluation tests for both the original and modified elements are included in Fig. B-2a.

Static pressures were sensed indirectly by measuring the wakes behind 1/4-in. diameter brass balls. Over a considerable range in Reynolds number, the pressure coefficient in the wake of a sphere is essentially constant through an angular range of 140 degrees. Evaluation tests on the individual sensing element are shown in Fig. B-2b. Static pressures are computed as follows:

$$p_T = p_S + 1/2\rho\, u^2$$

$$k = \frac{p_S - p_W}{1/2\rho\, u^2} = \frac{p_S - p_W}{p_T - p_S}$$

$$p_S = \frac{k\, p_T + p_W}{k + 1}$$

or

$$(p_S - p_o) = \frac{k(p_T - p_o) - (p_o - p_W)}{k + 1}$$

In the above equations, p_T = local total pressure,
p_S = local static pressure,
u = local velocity,
p_W = wake pressure, and
p_o = pressure at infinity.

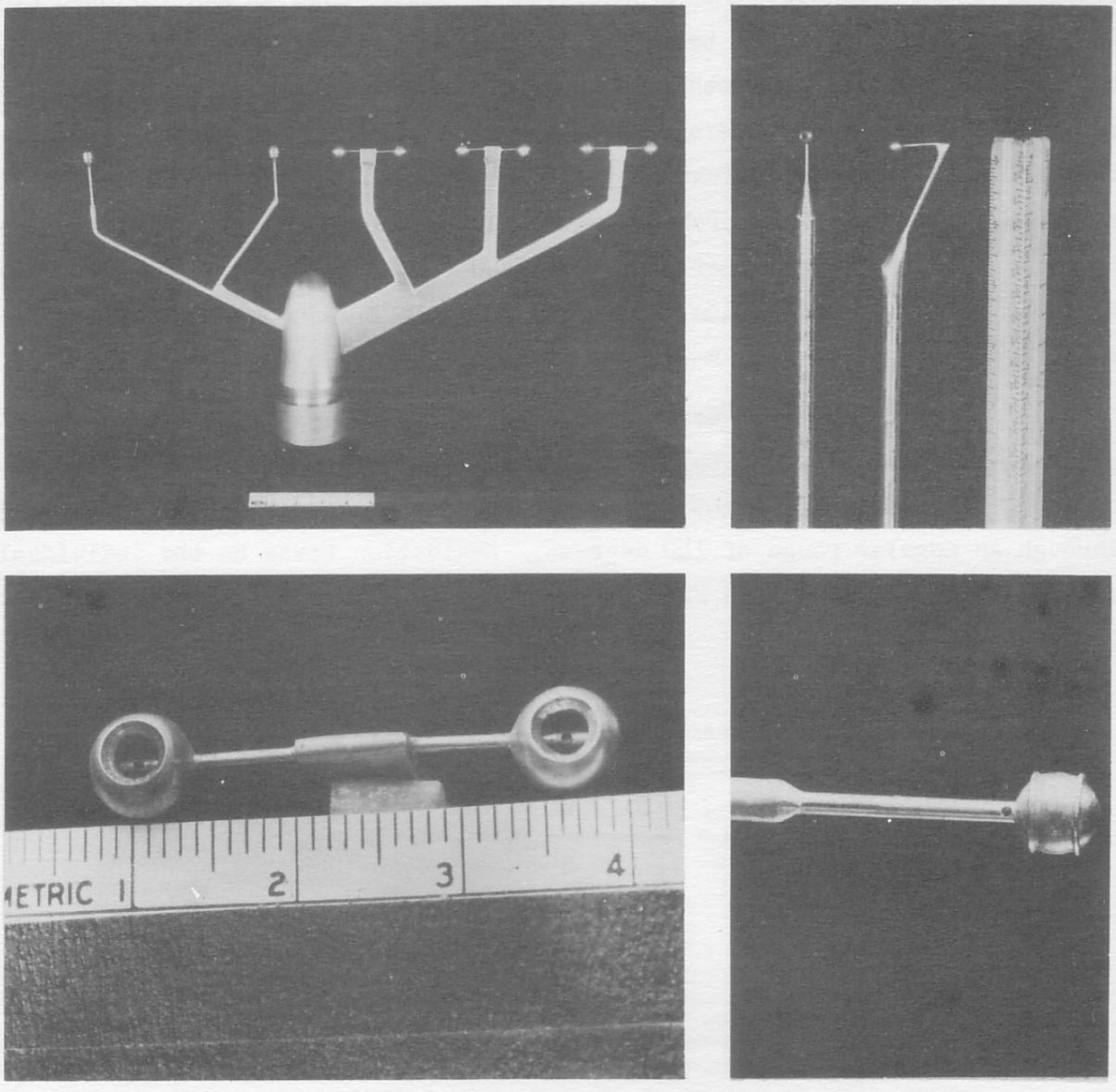

Fig. B-1 - Pressure Sensing Elements

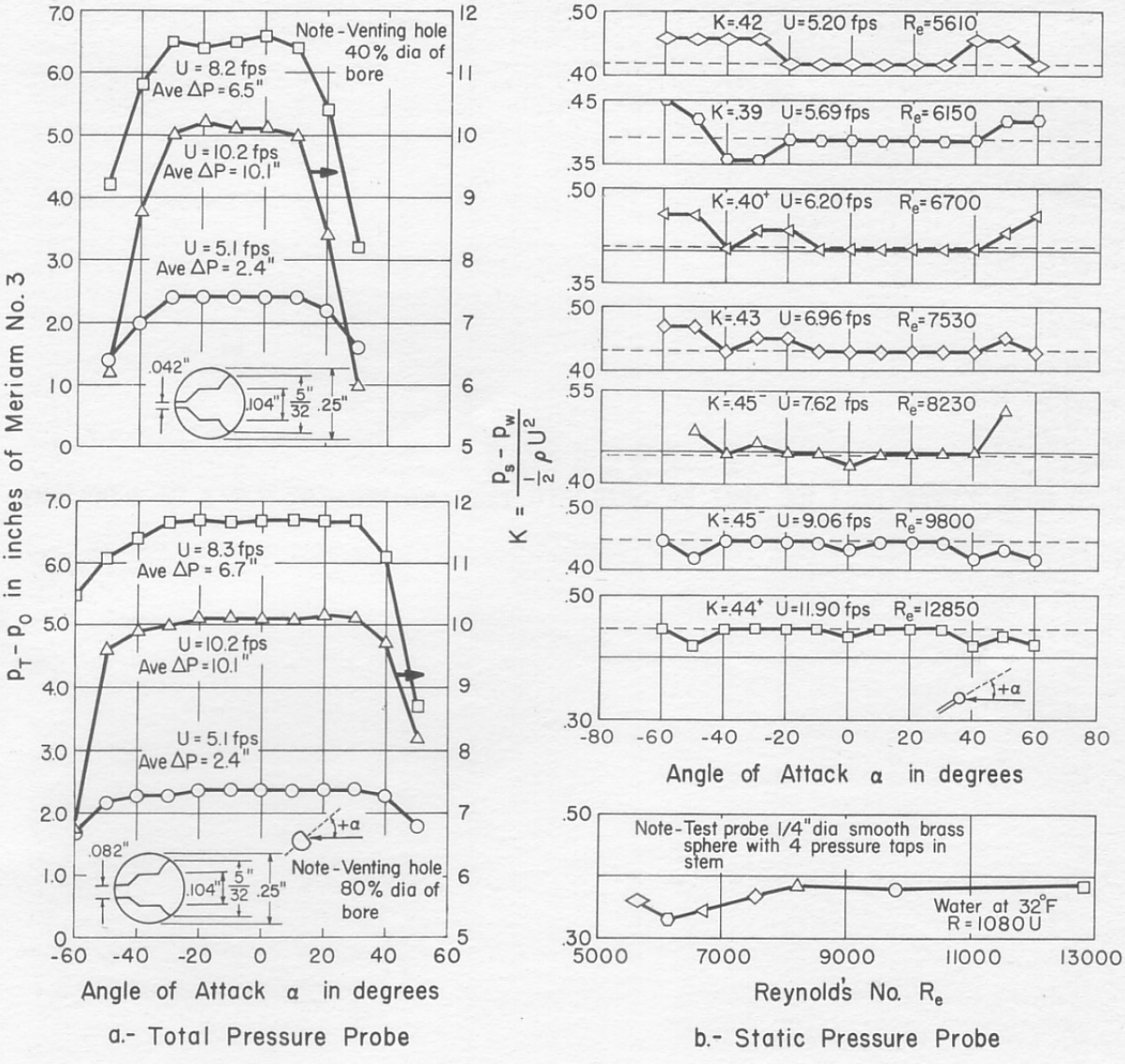

Fig. B-2 - Effect of Attack Angle on Total and Static Pressure Sensing Elements

APPENDIX C

ANALYSIS OF A TWO-DIMENSIONAL JET DISCHARGING INTO AN INFINITELY WIDE STREAM

APPENDIX C

ANALYSIS OF A TWO-DIMENSIONAL JET DISCHARGING INTO AN INFINITELY WIDE STREAM

In his treatment of this problem, Ehrich [7] has considered the velocity along the free streamline the same as the velocity at infinity. This assumption permitted a rational analysis for the irrotational flow case. Such a solution is physically unrealistic because the main stream is displaced and the eddy behind the jet extends an infinite distance. Further, it is intuitively apparent that a velocity field exists about the jet and the main stream flow is accelerated adjacent to the jet.

In order to render this problem tractable to rational analysis, it is suggested that a negative image jet (or sink) be placed a distance downstream equal to the eddy length. This is akin to the image method of Riabouchinsky for cavitation problems about plates. The flow pattern is rendered symmetrical and an analytic solution is possible for the case of the jet and free stream under the same total pressure.

The usual assumptions of an incompressible, irrotational flow are assumed. The physical plane with the reflected jet and the other mapping planes are shown in Fig. C-1. The origin in the physical plane is chosen at point E'.

The transformations are

$$W = -\frac{Q_j}{\pi}\left[\ell n \frac{\zeta + \ell}{\zeta - \ell} + \frac{\ell}{m^2 - \ell^2}(2\zeta) + i\pi\right] \qquad (C\text{-}1)$$

$$\frac{dQ}{d\zeta} = \frac{-iK}{(m^2 - \zeta^2)\sqrt{1 - \zeta^2}} \qquad (C\text{-}2)$$

Integrating and evaluating the constants at E' and the point of symmetry P gives

$$Q = -1/2 \ell n \frac{m\sqrt{\zeta^2 - 1} - \zeta\sqrt{m^2 - 1}}{m\sqrt{\zeta^2 - 1} + \zeta\sqrt{m^2 - 1}} \qquad (C\text{-}3)$$

The constant m is determined at point A in terms of the velocities as

$$m = \frac{(U_1/U_\infty)^2 + 1}{2\,(U_1/U_\infty)} = \frac{\alpha + 1}{2\sqrt{\alpha}} \qquad \text{(C-4)}$$

where $\alpha = (U_1/U_\infty)^2$ and U_1 is the free streamline velocity along E'PD' in the physical plane.

Generally speaking, the stream velocity U_∞ and either the jet opening a or the discharge Q_j may be considered as known. The free streamline velocity U_1 depends upon the pressure in the wake. In the example given below an experimental value for this wake pressure is used. In a more general sense, it should be noted that the momentum of the jet in the Y direction is balanced by the pressures along the adjacent wall. By integrating pressures along this wall from $-\infty$ to the center of the eddy, the eddy length may be evaluated in terms of U_1 (or the wake pressure), U_∞, V_j, and a. The procedure for analytically determining the wake pressure and trajectory becomes one of trial and error. Various values should be assigned to m until the eddy length plotted analytically has the same value as that determined from momentum considerations.

Evaluation at K' gives the following value for ℓ

$$\ell = 1/2\,\frac{(\alpha + 1)(\beta + 1)}{\sqrt{(\alpha + \beta)(\alpha\,\beta + 1)}} \qquad \text{(C-5)}$$

where $\beta = (U_1/V_j)^2$.

Integration across the slot opening in the physical plane may be used as an indirect method for finding the relation between V_j and U_∞. This apparently is quite tedious.

Although the velocity in the jet may be slightly less than that in the main stream, equating these velocities is realistic and their resulting flow pattern should be a close approximation of the actual. With $V_j = U_\infty$

$$\ell = m\,\frac{\alpha + 1}{\sqrt{2(\alpha^2 + 1)}} \qquad \text{(C-6)}$$

The equation for the free streamline E'P may be evaluated in parametric form in terms of its slope as follows:

$$x = \int_{\pi/2}^{\theta} \cos\theta ds \quad \text{and} \quad y = \int_{\pi/2}^{\theta} \sin\theta ds \tag{C-7}$$

in which $ds = -\frac{1}{U_1}\frac{d\phi}{d\theta}d\theta$.

Along E'P, the velocity is constant and from $Q = i\theta$ it can be shown that

$$\zeta = \frac{-m \sin\theta}{\sqrt{m^2 - \cos^2\theta}} \tag{C-8}$$

Hence, ϕ the real part of W becomes

$$\phi = -\frac{Q_j}{\pi}\left[\ell n \frac{\ell\sqrt{m^2 - \cos^2\theta} - m\sin\theta}{\ell\sqrt{m^2 - \cos^2\theta} + m\sin\theta} - \frac{2\ell m \sin\theta}{(m^2 - \ell^2)\sqrt{m^2 - \cos^2\theta}}\right]$$

Differentiating and substituting in Eq. (C-7) result in

$$x = \frac{Q_j}{U_1\pi} 2\ell m (m^2 - 1)\left[\int_{\pi/2}^{\theta} \frac{\cos^2\theta d\theta}{\sqrt{m^2 - \cos^2\theta}\,[\ell^2(m^2 - \cos^2\theta) - m^2\sin^2\theta]} + \right.$$

$$\left. \frac{1}{m^2 - \ell^2} \int_{\pi/2}^{\theta} \frac{\cos^2\theta d\theta}{(m^2 - \cos^2\theta)^{3/2}}\right] \tag{C-9}$$

The writer was not successful in integrating this expression and a numerical method was used for evaluation. It is noted that as $\ell \to 1$,

$$x \to -\frac{Q}{U_1\pi} 2m^3 \int_{\pi/2}^{\theta} \frac{d\theta}{(m^2 - \cos^2\theta)^{3/2}}$$

The integrated expression for y is

$$y = \frac{Q_j}{\pi U_1} 2\ell m \frac{m^2 - 1}{m^2 - \ell^2} \left[\sqrt{\frac{m^2 - \ell^2}{m^2(m^2 - 1)}} \tanh^{-1} \sqrt{\frac{(m^2 - \ell^2)(m^2 - \cos^2\theta)}{m^2(m^2 - 1)}} - \frac{1}{\sqrt{m^2 - \cos^2\theta}} \right]_{\pi/2}^{\theta} \qquad \text{(C-10)}$$

In Fig. C-2 a reproduction of data presented by Rouse on slot jets is shown. In this, he gives the empirical relation

$$L/B = 20\ (V/U)^{3/2} \qquad \text{(C-11)}$$

in which L is the eddy length and $B = a$, the slot width. Rouse's symbols V and U correspond respectively to V_j and U_∞. For $V_j = U_\infty$, $L/B = 20$ and the wake pressure is approximately

$$-0.6 \frac{\rho U^2}{2}.$$

Using these data, m is readily evaluated by equating total energies at A and P.

$$1/2\rho\ U_\infty^2 = 1/2\rho\ U_1^2 - 0.6\rho \frac{U_\infty^2}{2}$$

$$\alpha = (U_1/U_\infty)^2 = 1.6 \quad \text{and} \quad m = 1.028$$

The computed curve is shown in Fig. C-3. The solid lines represent the computed free streamline curve and the sketched-in penetration depth of the jet. A comparison is made with Rouse's data and Ehrich's computations as well as the penetration taken from Fig. 4. The pantographed trajectory of one photograph of a circular jet at $m = 1$ is also shown.

As seen from the curve, the maximum computed eddy height of $2.83a$ compares quite well with Rouse's value of approximately $3.1a$. The latter

value is taken from the H/L curve in Fig. C-2 in which H is the measured maximum eddy height. There was remarkable agreement on the location of this maximum eddy height, i.e., L/2 = 10a compared with the computed value L/2 = 10.07a.

It is surprising to note the agreement between the penetration data for three-dimensional jets and the two-dimensional theoretical line. The rapid flattening of the circular jet apparently lends it a two-dimensional character.

This type of analysis provides a method for predicting eddy length, maximum height, and the complete profile based on the premise that both flows are under the same total head, or that they have the same source at infinity. It may be remarked that placing image jets in a similar manner in a channel of finite width renders tractable the problem of a jet impinging into such a channel.

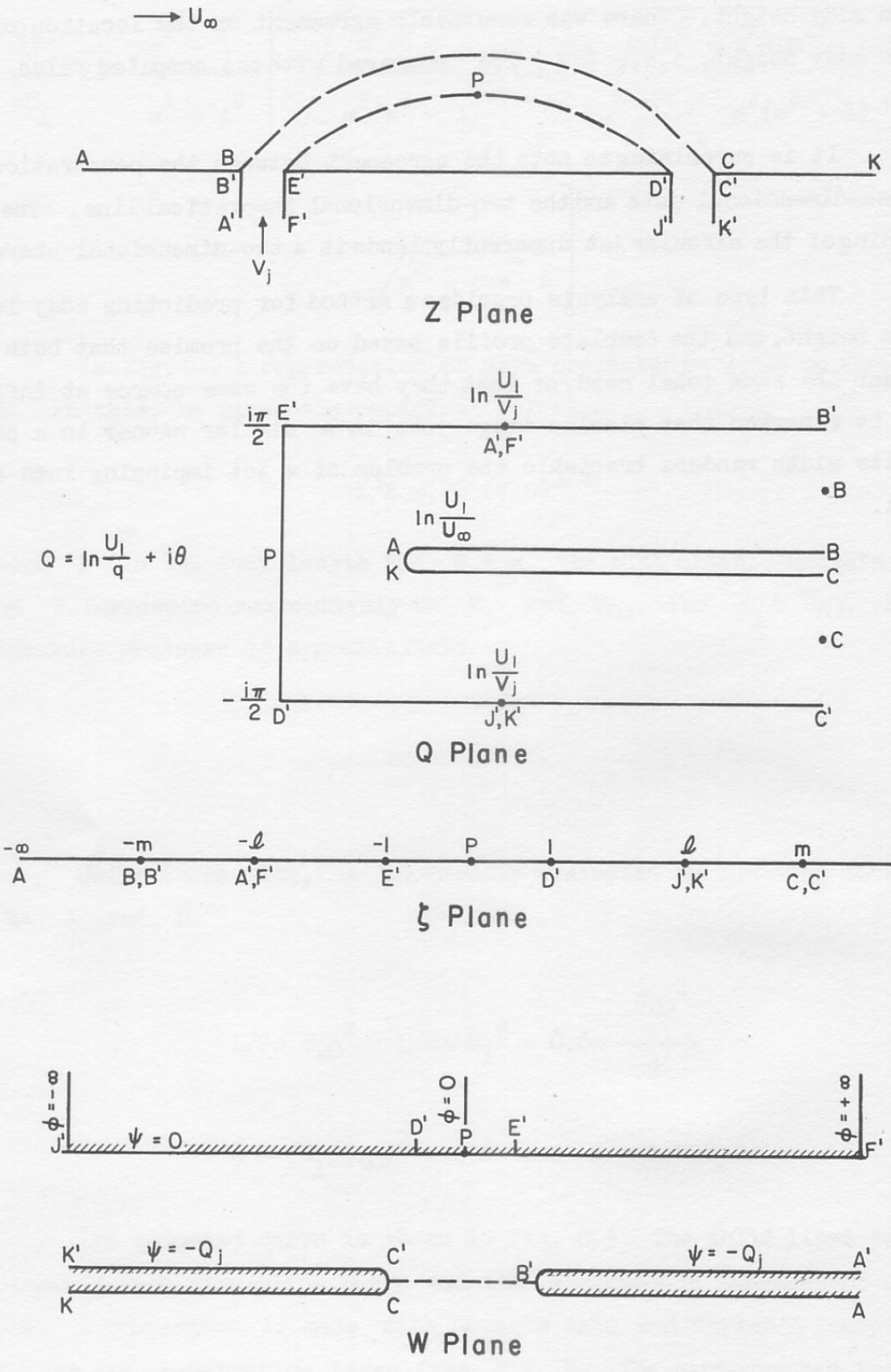

Fig. C-1 - Mapping Planes for Two-Dimensional Jet

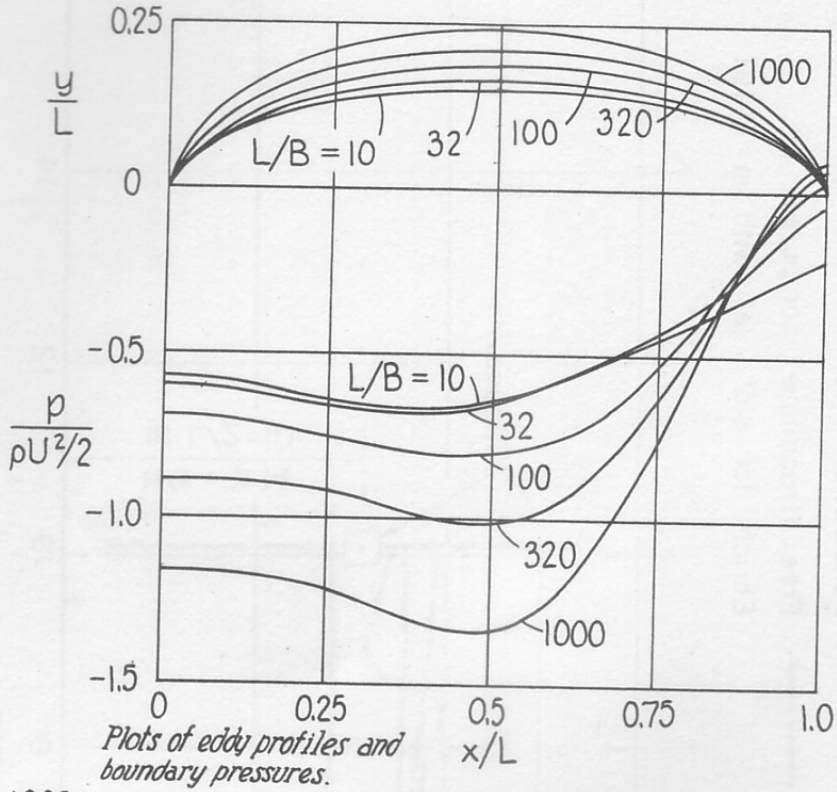

Plots of eddy profiles and boundary pressures.

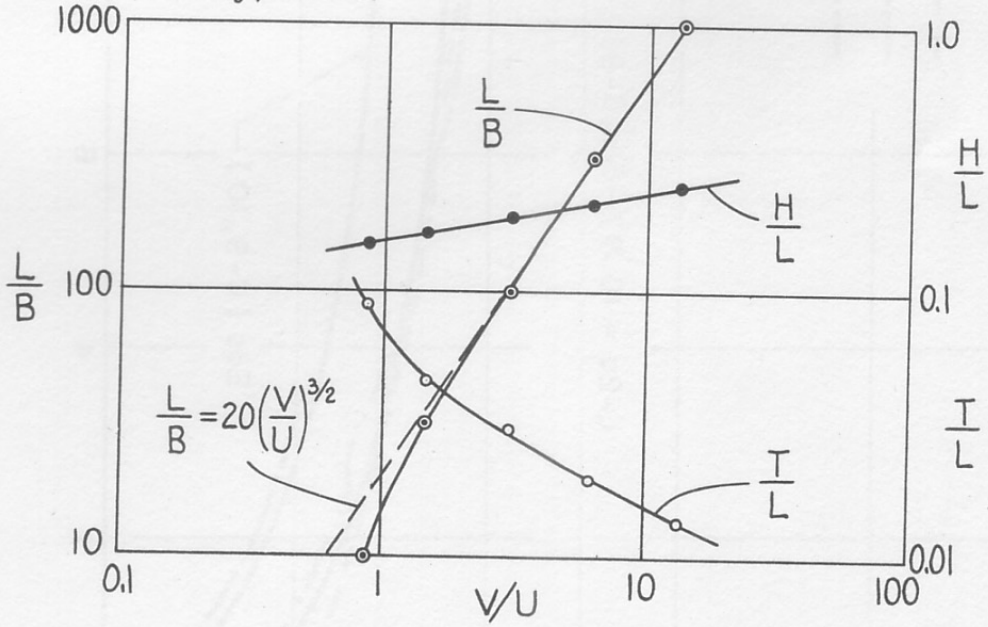

L/B, H/L and T/L as functions of V/U.

Fig. C-2 - Pressures in Wake of Two-Dimensional Jet
(Reprinted from Reference [15])

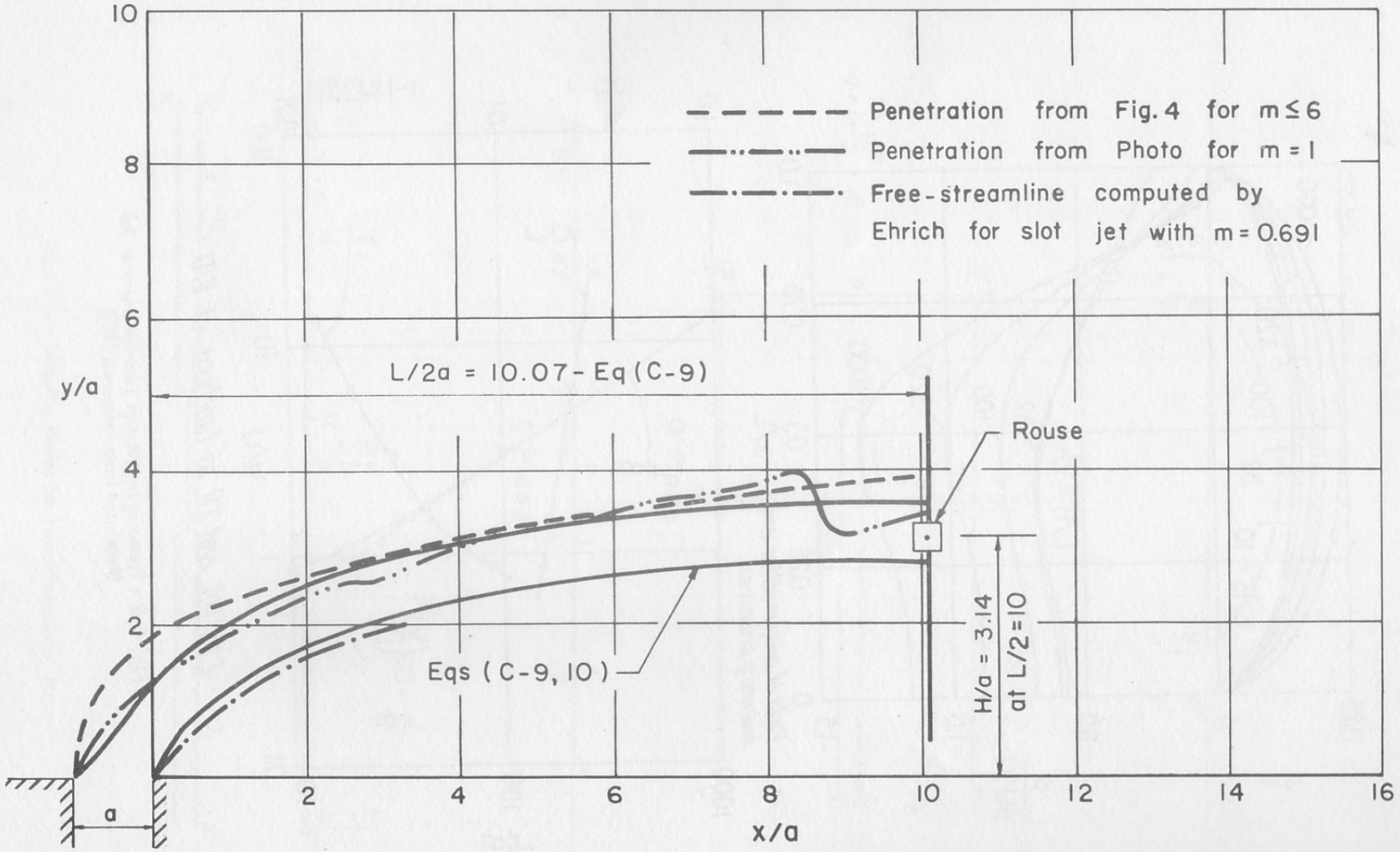

Fig. C-3 - Comparison of Slot and Circular Jets

DISTRIBUTION LIST FOR TECHNICAL PAPER NO. 28-B

of the St. Anthony Falls Hydraulic Laboratory

Copies	Organization
100	Commanding Officer and Director, David Taylor Model Basin, Washington 7, D. C., Att: Code 513.
9	Chief, Bureau of Ships, Department of the Navy, Washington 25, D. C. 5 - Technical Information Section (Code 335) 1 - Technical Assistant to Chief of the Bureau (Code 106) 1 - Preliminary Design (Code 420) 1 - Hull Design (Code 440) 1 - Research and Development Program Planning (Code 330)
6	Chief, Bureau of Yards and Docks, Department of the Navy, Washington 25, D. C.
2	Chief, Bureau of Aeronautics, Department of the Navy, Washington 25, D. C., Att: 1 - Aero and Hydro Branch (Code AD-3) 1 - Research Division (Code RS)
2	Chief, Bureau of Ordnance, Department of the Navy, Washington 25, D. C., Att: 1 - Assistant for Aero, Hydro, and Ballistics (Code Re03) 1 - Underwater Missile Branch (Code ReU1)
3	Chief of Naval Research, Department of the Navy, Washington 25, D. C., Att: Mechanics Branch (Code 438).
1	Director, U. S. Naval Research Laboratory, Washington 25, D. C., Att: Code 2021.
1	Commanding Officer, Office of Naval Research, Branch Office, The John Crerar Library Building, 10th Floor, 86 East Randolph Street, Chicago 1, Illinois.
1	Commander, U. S. Naval Ordnance Laboratory, White Oak, Silver Spring, Maryland.
1	Commander, U. S. Naval Ordnance Test Station, 3202 East Foothill Boulevard, Pasadena, California.
1	Commanding Officer and Director, U. S. Navy Underwater Sound Laboratory, Fort Trumbull, New London, Connecticut.
1	Superintendent, U. S. Naval Postgraduate School, Monterey, California, Att: Librarian.
1	Chief of Research and Development, Department of the Army, Washington 25, D. C.

Copies	Organization
1	Director, U. S. Waterways Experiment Station, P. O. Box 631, Vicksburg, Mississippi.
1	Office of the Chief of Engineers, Department of the Army, Gravelly Point, Washington 25, D. C.
5	Director, National Aeronautics and Space Administration, 1512 H Street, N. W., Washington 25, D. C.
1	Director, Langley Research Center, NASA, Langley Field, Virginia.
1	Director, Lewis Research Center, NASA, 21000 Brookpark Road, Cleveland 35, Ohio.
1	Director, Hydraulic Laboratory, Bureau of Reclamation, Denver Federal Center, Denver, Colorado.
5	Commander, Armed Services Technical Information Agency, Arlington Hall Station, Arlington 12, Virginia, Att: TIPDR.
2	Director, National Bureau of Standards, National Hydraulic Laboratory, Washington 25, D. C.
2	Newport News Shipbuilding and Dry Dock Company, Newport News, Virginia. For distribution as follows: 1 - Assistant Naval Architect 1 - Director, Hydraulics Laboratory
1	Chief, Engineering Research Division, Colorado State University, Fort Collins, Colorado.
1	California Institute of Technology, Division of Engineering, Pasadena 4, California, Att: Dr. M. S. Plesset, Professor of Applied Mechanics.
2	Dr. John Breslin, Davidson Laboratory, Stevens Institute of Technology, 711 Hudson Street, Hoboken, New Jersey.
1	Professor L. J. Hooper, Director, Alden Hydraulic Laboratory, Worcester Polytechnic Institute, Worcester 2, Massachusetts.
1	Dr. A. T. Ippen, Director, Hydrodynamics Laboratory, Massachusetts Institute of Technology, Cambridge 39, Massachusetts.
1	Professor Laurens Troost, Head, Department of Naval Architecture and Marine Engineering, Massachusetts Institute of Technology, Cambridge 39, Massachusetts.
1	Director, Woods Hole Oceanographic Institute, Woods Hole, Massachusetts, Att: Dr. C. O. Iselin, Senior Oceanographer.

Copies	Organization
1	Dean M. P. O'Brien, Department of Engineering, University of California, Berkeley 4, California.
1	Dr. Hunter Rouse, Director, Iowa Institute of Hydraulic Research, State University of Iowa, Iowa City, Iowa.
1	S. Logan Kerr and Company, 1520 Bethelehem Pike, Flourton, Pennsylvania, Att: Mr. S. Logan Kerr.
1	Allis Chalmers Company, Milwaukee, Wisconsin, Att: Mr. Wm. J. Rheingans.
1	Director, Engineering Societies Library, 29 West 39th Street, New York 18, New York.
2	Library, California Institute of Technology, Pasadena, California.
1	Librarian, Massachusetts Institute of Technology, Cambridge 39, Massachusetts.
2	Librarian, Library of Congress, Washington 25, D. C.
1	Librarian, School of Engineering, University of Texas, Austin, Texas.
2	Director, Ordnance Research Laboratory, Pennsylvania State University, University Park, Pennsylvania.
3	Serials Division, University of Minnesota Library, Minneapolis, Minnesota.
1	Dr. W. D. Baines, Head, Hydraulic Laboratory, National Research Council, Ottawa, Ontario, Canada.
1	Director, Netherlands Ship Model Basin, Haagsteeg 2, Wageningen, The Netherlands.
1	Director of Research, British Shipbuilding Research Association, 5 Chesterfield Gardens, Curzon Street, London, W1, England.
1	Dr. H. W. Lerbs, Director, Hamburg Model Basin, Branfelder Str. 164, Hamburg 33, Germany.
1	Dr. Hans Edstrand, Director, Statens Skeppsprovningsanstalt, 14 Gibraltargatan, Göteborg C, Sweden.
1	Professor J. K. Lunde, Director, Skipsmodelltanken, Skipsbygging, Trondheim, Norway.
1	Mr. M. G. Hiranandani, Director, Central Water and Power Research Station, 20 Bombay Poona Road, Poona 3, India.
1	Directeur, Bassin d'Essais des Carènes, 6, Boulevard Victor, Paris XVe, France.

Copies	Organization
1	Director, Canal de Experiencias Hidrodinamicas, Carretera de la sierra, El Pardo, Madrid, Spain.
1	Presidenza, Italian Model Basin, Via della Vasca Navale 89, Roma-Seda, Italy.
1	Chief of Cavitation Tunnel, Werkstad, Aktiebolaget Karlstads, Mechaniska, Kristinehamn, Sweden.
1	Mr. R. Jordinson, Northampton College of Advanced Technology, St. John St. E. C. 1, London, England.